Employing ternary fission of ^{242}Pu as a probe of very neutron-rich matter

J. B. Natowitz

Cyclotron Institute, Texas A&M University, College Station, Texas 778431, USA

H. Pais[*]

CFisUC, Department of Physics, University of Coimbra, 3004-516 Coimbra, Portugal

G. Röpke

Institute of Physics, University of Rostock, 18059 Rostock, Germany

Detailed assessments of the ability of recent theoretical approaches to modeling existing experimental data for ternary fission confirm earlier indications that the dominant mode of cluster formation in ternary fission is clusterization in very neutron-rich, very low-density, essentially chemically equilibrated nucleonic matter. An extended study and comparison of these approaches applied to ternary fission yields in the thermal neutron induced reaction ^{241}Pu(n_{th}, f) has been undertaken to refine the characterization of the source matter. The resonance-gas approximation has been improved taking in-medium effects on the binding energies into account. A temperature of 1.29 MeV, density of 6.7×10^{-5} nucleons/fm^3 and proton fraction $Y_p = 0.035$ are found to provide a good representation of yields of the ternary emitted light particles and clusters. In particular, results for $Z = 1$ and 2 isotopes are presented. Isotopes with larger Z are discussed, and the roles of medium and continuum effects, even at very low density, are illustrated.

I. INTRODUCTION

In the neutron induced or spontaneous ternary fission of a heavy isotope a nucleon or light cluster is emitted perpendicular to the fission axis determined by the two separating large fission fragments [1–11]. ^{4}He, emitted in approximately 1/500 events is the most dominant charged particle but other charged isotopes with charge number $Z = 1$ up to $Z = 18$ have been observed [9,10]. These light charged particles (LCP) are emitted from the neck region at the time of scission and may be considered as signals, which describe the state of nuclear matter in the neck at that time.

To interpret the observed ternary yields, statistical models have been applied, which assume thermodynamic equilibrium at chemical freezeout during scission [12–14]. However, experimental yields for the heavier elements are typically overestimated unless some mechanism for suppression of higher mass products is introduced [13,14]. In Wuenschel *et al.* [14], chemical equilibrium is achieved in accordance with the grand canonical ensemble only for the lightest isotopes and a time-dependent nucleation process for production of heavier LCP is introduced [15,16] so that the LCP yield becomes increasingly suppressed with increasing mass number.

Recently, this approach has been explored in more detail and used to determine isotopic equilibrium constants

for LCP emitted in the ternary fission reaction ^{241}Pu(n_{th}, f) [17]. Further investigations were then undertaken to better characterize the ternary fissioning ^{242}Pu source. In Ref. [18], the simple ideal model of nuclear statistical equilibrium was improved considering medium effects and continuum correlations [19], e.g., resonances such as ^{4}H, ^{5}He, ^{8}Be (as known from the virial expansion of the nuclear matter equation of state). A nearly perfect description of the measured yields of H and He isotopes for ^{252}Cf(sf) was obtained. In Ref. [20], several different fission reactions were investigated within an information entropy approach, and isotopes up to $Z = 6$ are included. These investigations showed that the dominant mode of cluster formation in ternary fission is clusterization in very neutron-rich, very low-density, essentially chemically equilibrated nucleonic matter at temperatures near 1 MeV.

In the present work, an extended study and comparison of the different approaches applied to modeling ternary fission yields in the thermal neutron induced reaction ^{241}Pu(n_{th}, f) [9,10] is undertaken. A more detailed exploration of the in-medium and continuum effects leads to a more refined characterization of the source matter. We show that, in particular, the weakly bound states are strongly influenced by in-medium effects and provide an alternative observable to determine the density of the source matter. We find that the neck matter at scission has a temperature $T \approx 1.29$ MeV, a nucleon density $n_B \approx 6.7 \times 10^{-5}$ nucleons/fm^3, and a proton fraction $Y_p \approx 0.035$. This work provides a baseline laboratory test of the low-density nuclear equation of state for conditions,

which may be encountered in astrophysical sites such as core-collapse supernova events in which a neoneutron star is formed, evolves with time and cools down to a neutron star [21]. Similar neutron-rich matter may also be produced in the merging of a binary neutron star system. Both systems relax to a temperature of about 1 MeV in less than a minute. In such dense, highly excited systems, surface densities of 10^{11} g/cm^3 are typical, but the proton fraction may be different. In β equilibrium, it depends upon the neutrino density, see, e.g., Refs. [22,23]. Even if the proton fraction in astrophysical scenarios is different from the proton fraction in the neck matter at scission, the equations of state (for a review see, e.g., Refs. [24,25]) employed over a wide region of parameter values may be checked at the special conditions of scission. Investigations of the correct description of correlations under scission conditions may also be applied to other regions of the astrophysical parameter space.

II. YIELDS FROM A QUANTUM STATISTICAL APPROACH

We consider different stages of the fission process. For the time evolution of the nucleonic system up to scission we assume a quick relaxation to local thermodynamic equilibrium. Within the statistical model framework the grand canonical distribution at scission, where chemical freezeout takes place, gives the primordial (or primary) yields for the relevant species. For the time evolution after scission we assume a reaction kinetics in which populated excited states decay, and the kinetic energies are determined by the interaction between the fission products. The decay of unstable nuclear states and resonances is described as feed-down processes, which transform the primordial distribution of yields to the final observable yield distribution. This approach to the time evolution of the fission process may be considered as an approximation within the systematic approach of nonequilibrium statistical operators where both stages of time evolution, the hydrodynamical and kinetic ones, are unified within an information theoretical approach [18,20]. This information theoretical approach allows us to introduce Lagrange parameters $\lambda_T(t)$, $\lambda_n(t)$, $\lambda_p(t)$, which are the nonequilibrium generalizations of the temperature and the chemical potentials of neutrons (n) and protons (p). They depend on time t and, in general for the hydrodynamical description, also on position.

In the present work, we focus on inferring the corresponding Lagrange parameters λ_i for the primary distribution at chemical freezeout from the observed final yield distribution. For this, we need an accurate solution of the grand canonical distribution at scission. We employ and compare three successive approximations:

(i) The resonance-gas approximation (res.gas) known also as nuclear statistical equilibrium (NSE), see Refs. [25,26] where the nucleonic system is considered as an ideal mixture of nuclei in the ground state and in (unstable) excited states and resonances. A semiempirical improvement is the excluded volume model [27,28].

(ii) The virial approximation (vir) where binary interactions between the different constituents are taken into account considering the respective scattering phase shifts [26,29,30].

(iii) Accounting for in-medium corrections (medium) such as self-energy shifts and Pauli blocking effects [26,31,32].

In particular, we investigate whether the frequently used nuclear statistical equilibrium model is sufficient to describe nucleonic systems under the scission conditions in the neck region or whether continuum correlations and in-medium effects must be taken into account.

In the quantum statistical (QS) approach, after the cluster decomposition of the spectral function, the density is decomposed into partial densities of different channels characterized by A, Z [18]. The primordial yields, here denoted as relevant yields $Y_{A,Z}^{\mathrm{rel,approx}}$, are calculated in the corresponding approximation as

$$Y_{A,Z}^{\mathrm{rel,approx}} \propto R_{A,Z}^{\mathrm{approx}} \, g_{A,Z} \left(\frac{2\pi\hbar^2}{Am\lambda_T} \right)^{-3/2}$$
$$\times \, e^{(B_{A,Z}+(A-Z)\lambda_n+Z\lambda_p)/\lambda_T}, \quad (1)$$

where $B_{A,Z}$ denotes the (ground-state) binding energy and $g_{A,Z}$ the degeneracy [33]. The prefactor

$$R_{A,Z}^{\mathrm{approx}} = 1 + \sum_i^{\mathrm{exc}} [g_{AZ,i}/g_{A,Z}] e^{-E_{AZ,i}/\lambda_T} \quad (2)$$

is related to the intrinsic partition function of the cluster $\{A, Z\}$.

Different approximations are considered for the intrinsic partition function as discussed above.

(i) In the resonance-gas approximation, the summation for $R_{A,Z}^{\mathrm{res.gas}}(\lambda_T)$ is performed over all excited states i, excitation energy $E_{AZ,i}$, and degeneracy $g_{AZ,i}$ [33].

(ii) In the virial approximation, $R_{A,Z}^{\mathrm{vir}}(\lambda_T)$, the summation in (2) is performed over all excited states i, which are bound. Also, the continuum contributions are included. For instance, the Beth-Uhlenbeck formula expresses the contribution of the continuum to the intrinsic partition function via the scattering phase shifts, see Refs. [18,19,29–31,34].

(iii) The expression $R_{A,Z}^{\mathrm{medium}}(\lambda_T, \lambda_n, \lambda_p)$ takes in-medium effects into account, in particular the shifts of binding energy values because of self-energy, Pauli blocking effects and the modification of bound-state wave functions and scattering phase shifts. Therefore, this term is also dependent on the densities of neutrons and protons.

A simple statistical equilibrium distribution, where for each isotope $\{A, Z\}$ only the ground state is taken into account, is obtained for $R_{A,Z}^{\mathrm{approx}}(\lambda_T) = 1$, i.e., neglecting the contribution of all excited states including continuum correlations. Details to evaluate the intrinsic partition function and $R_{A,Z}^{\mathrm{res.gas}}, R_{A,Z}^{\mathrm{vir}}, R_{A,Z}^{\mathrm{medium}}$ are presented for $Z \leqslant 6$ in the Appendix.

As an example we focus on the fission reaction ^{241}Pu(n_{th}, f) induced by thermal neutrons where good data for the ternary fission yields are available [9,10]. The observed yields up to ^{20}C are shown in Tables I, II below. Instead of normalizing to the yield of total α particle emission, assigned to be 10000, we employ absolute yields per fission. The total α particle emission yield per fission was taken from Ref. [4].

The Koester data do not contain values for scission nucleon (n or p) emission. Determination of those yields is

TABLE I. Observed yields per fission of ternary fission of ^{241}Pu(n_{th}, f), including 0.107 for scission neutrons (col. 4), are compared to a final-state distribution, calculated in the resonance-gas approximation. The Lestone fit metric [13] is calculated for the isotopes with $Z \leqslant 2$. The minimum is found for the parameter values given at the end of table. $Y_{A,Z}^{\text{rel,res.gas}}$ denotes primordial yield, $Y_{A,Z}^{\text{final,res.gas}}$: final yield, $X_{A,Z}^{\text{res.gas}} = A Y_{A,Z}^{\text{res.gas}} / \sum_{A',Z' \leqslant 2} A' Y_{A',Z'}^{\text{res.gas}}$: mass fraction.

isotope	A	Z	$Y_{A,Z}^{\text{obs}}$	$R_{A,Z}^{\text{res.gas}}(1.29)$	$Y_{A,Z}^{\text{rel,res.gas}}$	$Y_{A,Z}^{\text{final,res.gas}}$	$X_{A,Z}^{\text{res.gas}}$
1n	1	0	0.107	1	0.1098	0.1098	0.9215
1H	1	1	–	1	4.298×10^{-6}	4.298×10^{-6}	0.00003414
2H	2	1	8.463×10^{-6}	1	8.889×10^{-6}	8.889×10^{-6}	0.000146
3H	3	1	1.584×10^{-4}	1	1.212×10^{-4}	1.398×10^{-4}	0.00359
4H*	4	1	–	1.579	1.855×10^{-5}	[→ ^{3}H]	–
3He	3	2	–	1	2.549×10^{-9}	2.817×10^{-9}	6.163×10^{-8}
4He	4	2	2.015×10^{-3}	1	1.449×10^{-3}	1.911×10^{-3}	0.06529
5He*	5	2	–	1	3.999×10^{-4}	[→ ^{4}He]	–
6He^0	6	2	5.239×10^{-5}	1	4.322×10^{-5}	5.916×10^{-5}	0.003232
6He*	6	2	–	1.242	5.407×10^{-5}	[→ ^{4}He]	–
7He*	7	2	–	1.156	1.594×10^{-5}	[→ ^{6}He]	–
8He	8	2	3.022×10^{-6}	1	2.605×10^{-6}	2.898×10^{-6}	0.0002249
8He*	8	2	–	0.452	1.193×10^{-6}	[→ ^{4}He]	–
9He*	9	2	–	1.426	2.929×10^{-7}	[→ ^{8}He]	–
6Li	6	3	–	1	4.059×10^{-8}	4.059×10^{-8}	2.085×10^{-6}
6Li*	6	3	–	0.5471	2.46×10^{-8}	[→ ^{3}H]	–
7Li	7	3	1.35×10^{-6}	1.345	2.207×10^{-6}	2.545×10^{-6}	0.0001591
8Li	8	3	8.463×10^{-7}	1.281	1.357×10^{-6}	1.357×10^{-6}	0.00009983
8Li*	8	3	–	0.3151	3.374×10^{-7}	[→ ^{7}Li]	–
9Li	9	3	1.672×10^{-6}	1.062	2.181×10^{-6}	2.335×10^{-6}	0.0002005
10Li*	10	3	–	1	1.531×10^{-7}	[→ ^{9}Li]	–
11Li^0	11	3	9.068×10^{-10}	1	2.785×10^{-8}	2.962×10^{-8}	3.312×10^{-6}
12Li*	12	3	–	1	1.773×10^{-9}	[→ ^{11}Li]	–
7Be	7	4	–	1.359	2.382×10^{-11}	2.382×10^{-11}	1.401×10^{-9}
8Be*	8	4	–	1.477	1.59×10^{-6}	[→ ^{4}He]	–
9Be	9	4	8.866×10^{-7}	1	1.616×10^{-6}	1.616×10^{-6}	0.0001325
9Be*	9	4	–	0.5628	1.244×10^{-6}	[→ ^{4}He]	–
10Be	10	4	9.269×10^{-6}	1.367	1.112×10^{-5}	1.51×10^{-5}	0.001435
10Be^0	10	4	–	0.0789	6.553×10^{-7}	[→ ^{10}Be]	–
11Be^0	11	4	1.189×10^{-6}	1	2.422×10^{-6}	4.313×10^{-6}	0.0004634
11Be^0	11	4	–	0.7803	1.891×10^{-6}	[→ ^{11}Be]	–
11Be*	11	4	–	1.343	3.287×10^{-6}	[→ ^{10}Be]	–
12Be	12	4	5.642×10^{-7}	2.149	2.781×10^{-6}	3.73×10^{-6}	0.0004532
12Be^0	12	4	–	0.3657	7.655×10^{-7}	[→ ^{12}Be]	–
13Be*	13	4	–	1	1.84×10^{-7}	[→ ^{12}Be]	–
14Be	14	4	5.441×10^{-10}	1	3.606×10^{-8}	4.117×10^{-8}	6.237×10^{-6}
15Be*	15	4	–	1	5.114×10^{-9}	[→ ^{14}Be]	–

experimentally very challenging [6–8]. Experimental scission proton yields are very small and careful experiments have revealed that secondary processes dominate the apparent yields reported [6]. In our opinion the best available constraint on the scission proton yield is that of Ref. [6], where only an upper limit of 2.9–4.0 × 10^{-5} is deduced. Interestingly, although the determination of scission neutron emission yield in the presence of a much larger yield of secondary neutrons evaporated from the separated fission fragments is inherently even more difficult, very precise measurements and analyses of the neutron energy and angular distributions have been carried out and lead to the conclusion that the scission neutron yield is 0.107 per fission, approximately one-thirtieth of the total neutron yield [7,8]. We have adopted this number for our analysis. It is worth noting that, in an equilibrium picture,

the relative scission neutron and proton yields implied by these results indicate that the neck matter at scission is extremely neutron rich. That this must be the case has previously been inferred from the fact that ^{3}He has not been detected in ternary fission experiments while the isotope ^{3}H, with a similar binding energy is the second most abundant ternary charged fragment observed [3,4].

The standard nuclear statistical equilibrium (NSE) approach describes matter in the low-density limit where interaction between the components may be neglected (ideal gas of nucleons and nuclei in ground and excited states). We suggest a consistent quantum statistical description of interacting components as done, for instance, for the equation of state [34]. In particular we take into account continuum correlations and in-medium effects.

TABLE II. Continuation of Table I. Observed yields per fission of ternary fission of ^{241}Pu(n_{th}, f) (col. 4) are compared to a final-state distribution, calculated in resonance-gas approximation, including 0.107 for scission neutrons. The Lestone fit metric is calculated for the isotopes with $Z \leqslant 2$. The minimum is found for the parameter values given at the end of table.

isotope	A	Z	$Y_{A,Z}^{obs}$	$R_{A,Z}^{res.gas}(1.29)$	$Y_{A,Z}^{rel,res.gas}$	$Y_{A,Z}^{final,res.gas}$	$X_{A,Z}^{res.gas}$
10B	10	5	–	1.363	2.484×10^{-9}	2.565×10^{-9}	2.295×10^{-7}
10B^0	10	5	–	0.0443	8.17×10^{-11}	[$\rightarrow$ ^{10}B]	–
11B	11	5	3.224×10^{-7}	1.175	8.876×10^{-7}	8.876×10^{-7}	0.00009106
12B	12	5	2.015×10^{-7}	2.251	1.703×10^{-6}	1.835×10^{-6}	0.0002126
12B^0	12	5	–	0.1715	1.32×10^{-7}	[$\rightarrow$ ^{12}B]	–
13B	13	5	–	1	4.367×10^{-6}	4.91×10^{-6}	0.0006411
14B^0	14	5	2.62×10^{-8}	1	1.123×10^{-6}	1.504×10^{-6}	0.0002177
14B^0	14	5	–	0.3381	3.809×10^{-7}	[$\rightarrow$ ^{14}B]	–
14B*	14	5	–	0.4803	5.426×10^{-7}	[$\rightarrow$ ^{13}B]	–
15B	15	5	9.269×10^{-9}	1	7.523×10^{-7}	7.691×10^{-7}	0.0001235
16B*	16	5	–	1	1.685×10^{-8}	[$\rightarrow$ ^{15}B]	–
17B	17	5	–	1	2.021×10^{-8}	2.26×10^{-8}	4.397×10^{-6}
18B*	18	5	–	1	2.389×10^{-9}	[$\rightarrow$ ^{17}B]	–
13C	13	6	–	1.358	2.079×10^{-6}	2.079×10^{-6}	0.0002587
14C	14	6	2.539×10^{-6}	1.069	4.479×10^{-5}	5.129×10^{-5}	0.007177
15C	15	6	8.665×10^{-7}	1	2.08×10^{-5}	5.606×10^{-5}	0.008647
15C^0	15	6	–	1.69	3.527×10^{-5}	[$\rightarrow$ ^{15}C]	–
15C*	15	6	–	0.3074	6.501×10^{-6}	[$\rightarrow$ ^{14}C]	–
16C	16	6	1.008×10^{-6}	2.272	6.149×10^{-5}	9.799×10^{-5}	0.01218
16C^0	16	6	–	0.885	2.425×10^{-5}	[$\rightarrow$ ^{16}C]	–
17C^0	17	6	1.29×10^{-7}	1	1.816×10^{-5}	4.693×10^{-5}	0.008776
17C^0	17	6	–	1.582	2.877×10^{-5}	[$\rightarrow$ ^{17}C]	–
17C*	17	6	–	0.6677	1.225×10^{-5}	[$\rightarrow$ ^{16}C]	–
18C	18	6	5.642×10^{-8}	3.172	3.515×10^{-5}	4.42×10^{-5}	0.009127
19C^0	19	6	5.038×10^{-10}	5.112	1.662×10^{-5}	1.662×10^{-5}	0.003715
19C*	19	6	–	2.776	9.051×10^{-6}	[$\rightarrow$ ^{18}C]	–
20C	20	6	7.254×10^{-10}	2.426	3.743×10^{-6}	3.743×10^{-6}	0.0009117
λ_T [MeV]				1.2897			
λ_n [MeV]				−3.1486			
λ_p [MeV]				−16.273			
volume [fm^3]				1859.4			
n_B [fm^{-3}]				0.000064			
Y_p				0.03486			
fit metric				0.005485			

III. EXTRACTION OF LAGRANGE PARAMETERS FROM OBSERVED YIELDS

In this section we demonstrate how the Lagrange parameters $\lambda_i = \{\lambda_T(t), \lambda_n(t), \lambda_p(t)\}$ may be extracted from the observed yields. For simplicity, we use in this example only the simplest approximation for the intrinsic partition function, i.e., the ideal resonance-gas approximation. $R_{A,Z}^{res.gas}(\lambda_T)$ is calculated according (2) where for isotopes $\{A, Z\}$ all excited states i are summed over, the excitation energies $E_{AZ,i}$ and angular momentum degeneracies $g_{AZ,i} = 2J_{AZ,i} + 1$ are taken from the nuclear data tables [33]. In the Appendix we give these values for $Z \leqslant 6$ as well as the ground-state binding energies and the threshold energies for the continuum of scattering states $E_{A,Z}^{thresh}$. In Tables IV–VIII, we divide the intrinsic partition function into different parts with respect to the contribution to the final yields: The summation over all excited states above the threshold energy is marked by an asterisk. After freezeout, these excited states are assumed to

decay and feed the yields of daughter isotopes observed in the final distribution. This process is also explained in Tables I, II, where in column 7 the respective feed-down channel is indicated. The other excited states are assumed to γ decay to the ground state and remain in the same isotope channel. Furthermore, we indicate by the superscript "0" the states that have a binding energy smaller than 1 MeV below the continuum threshold. These weakly bound states are of special interest when in-medium effects are considered.

We use this subdivision of the intrinsic partition function to model the kinetic stage of evolution, i.e., the transition from the primary distribution to the final distribution considering only decay processes of the excited nuclei. In a more general approach, this sharp subdivision should be replaced by branching ratios describing the feed down to the final yields or using reaction networks.

For the resonance-gas approximation and the virial approximation the R factors are functions of the temperaturelike parameter λ_T. If in-medium effects are taken into account, the

R factor depends in addition on the chemical potentials λ_n, λ_p. Within our fit procedure described below, they are determined self-consistently. With a given set of Lagrange parameters, we are able to calculate the primary yields and the final yields. This is shown for the resonance gas approximation in Tables I, II as well as in Tables IX, X where in-medium effects are taken into account. In each case the calculated final yields are compared with the observed yields.

The task is then to find values for the Lagrange parameters, which reproduce the observed yield in an optimum way. We have previously observed [14,18,20] that yields of isotopes with large mass number are suppressed because of nucleation kinetics or size effects. For the fission process ^{241}Pu$(n_{\text{th}}$, f) this suppression with respect to the grand canonical distribution is observed for $A > 10$. To avoid this effect we use only the charged particles up to $Z = 2$, i.e., the observed yields of ^{1}n, ^{2}H, ^{3}H, ^{4}He, ^{6}He, ^{8}He to find values for the Lagrange parameters. As shown in Ref. [20], the inclusion of further isotopes with $A \leqslant 10$ gives approximately identical Lagrange parameters λ_i.

As in Ref. [14], we use for the fit metric that of Lestone [13], defined by

$$M^2 = \frac{1}{\mathcal{N}} \sum_{A,Z}^{\mathcal{N}} \left(\ln \left[Y_{A,Z}^{\text{final,approx}} \right] - \ln \left[Y_{A,Z}^{\text{obs}} \right] \right)^2, \qquad (3)$$

where $\mathcal{N}$ is the number of fitted experimental data points.

As shown in Table II, the values $\lambda_T = 1.29$ MeV, $\lambda_n = -3.149$ MeV, and $\lambda_n = -16.273$ MeV are obtained from the minimum of the fit metric for the resonance-gas approximation. The fit metric is also given in Table II. From the yields per fission, we can also derive a volume. The baryon density n_B is obtained from the observed yields per fission $n_B = \sum_{A,Z} A Y_{A,Z}^{\text{obs}}$ divided by the volume, it is mainly determined by the neutron density. The proton fraction Y_p is obtained as $\sum_{A,Z} Z Y_{A,Z}^{\text{obs}} / n_B$, it is mainly determined by the yield of ^{4}He. There is an uncertainty because the free proton density is not included in the fit, but the calculated values $Y_{1,1}$ are small so that no large effect is expected if the contribution of ^{1}H is dropped.

The observed values ^{1}n$^{\text{obs}}$, ^{2}H$^{\text{obs}}$, ^{3}H$^{\text{obs}}$, ^{4}He$^{\text{obs}}$, ^{6}He$^{\text{obs}}$, and ^{8}He$^{\text{obs}}$ are well reproduced, the deviation of about 10% is within the experimental error limits. Below, in the next section, we will also discuss the isotopes with $Z > 2$.

The value for temperature is consistent with values previously obtained for thermal neutron and spontaneous fission [35,36]. The proton fraction is directly determined from summation of the ternary product scission yields, primarily from the yields of neutrons and ^{4}He. The value of the baryon density is debated, in our work it is to be determined as optimum to reproduce the measured yields. We calculate the composition assuming different values for the density to show that there is a strong variation of the composition and a sharp minimum of the fit metric.

A main result is the low value of the density $n_B = 6.4 \times 10^{-5}$/fm^3 in resonance-gas approximation. We performed the fit considering the isotopes with $Z \leqslant 2$. Larger LCP (metals) will be included below in Sec. IV. To show how sharp the fit value for the density is, we per-
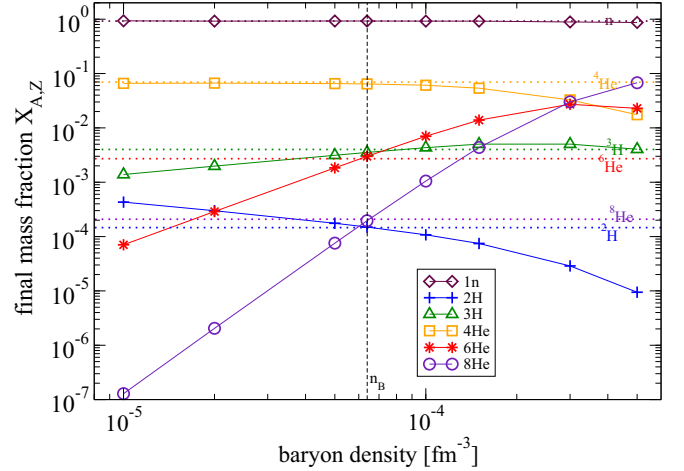

FIG. 1. Calculated light isotope yields (resonance-gas approximation) as a function of baryon density n_B (fixed temperature $T = 1.289$ MeV and proton fraction $Y_p = 0.0349$) for $Z = 1, 2$ isotopes (represented by symbols) are compared with the observed experimental yields represented by horizontal dotted lines. Optimum agreement based on a fit metric proposed by Lestone (3) is found at a density of $n_B = 6.4 \times 10^{-5}$ fm^{-3} (dashed line). See Fig. 2.

formed calculations for the composition, mass fraction $\tilde{X}_{A,Z} = A Y_{A,Z} / \sum_{A',Z' \leqslant 2} A' Y_{A',Z'}$, for fixed values of λ_T and proton fraction $\tilde{Y}_p = \sum_{A,Z \leqslant 2} Z Y_{A,Z} / \sum_{A,Z \leqslant 2} A Y_{A,Z}$ but variable density $\tilde{n}_B = \sum_{A,Z \leqslant 2} A Y_{A,Z}$, divided by the volume, see Fig. 1, where we compare the calculated values (final,res.gas) with the observed values (obs). (Note that the densities and proton fractions are calculated in the present section from the yields of n, H, and He isotopes, dropping the contributions of the metals.)

As indicated above, all calculations presented in this section were performed for the ideal resonance-gas approximation, the simplest of the three cases considered. The same calculations can be performed for the other approximations of the intrinsic partition function as shown below. With respect to the results discussed in the present section, no significant changes in the Lagrange parameters will be observed. However the successive approaches do reveal evidence for continuum and medium effects that even at this very low density, particularly for weakly bound and/or very neutron-rich isotopes.

The quality of the fit is expressed by the Lestone fit metric (3), see Fig. 2.

IV. INCLUSION OF HEAVIER ISOTOPES

We now consider the yields of isotopes with $2 < Z \leqslant 6$. For these elements, accurate values for observed yields of ternary fission are available for ^{241}Pu$(n_{\text{th}}$, f) [9,10]. For heavier elements $Z > 6$ calculations can be performed, but observed data become incomplete and less accurate.

For this purpose, we again calculate the relevant, primary distribution within a quantum statistical approach using the several different approximations proposed. In a first
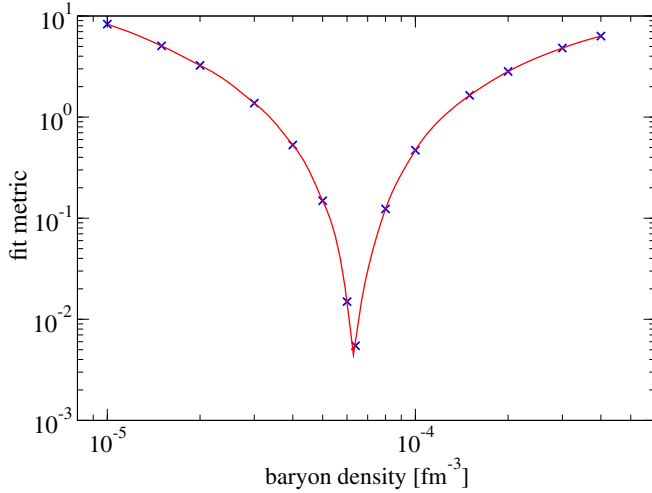
FIG. 2. Fit metric (3) vs. baryon density n_B for $T = 1.289$ MeV and $Y_p = 0.0349$.

FIG. 3. Ternary fission of ^{241}Pu(n_{th}, f): Ratios $Y_{A,Z}^{\text{obs}}/Y_{A,Z}^{\text{final,res.gas}}$ (bold symbols) and $Y_{A,Z}^{\text{obs}}/Y_{A,Z}^{\text{final,vir}}$ (full lines) as function of the mass number A. Isotopes with $Z \leqslant 6$ are shown. Data from Table III.

approximation of the ideal resonance gas, for each A, Z not only the ground state, but also all excited states are considered, which will give the intrinsic partition function. We take the excited states from the data tables [33] together with their degeneracy, see the Appendix, Tables IV–VIII. The possible decay to other isotopes is also indicated. For this, the threshold energy E_{AZ}^{thresh} is given where the decay channels open, in general the separation energy S_n for neutrons, but also other possible decay channels such as for ^{7}Li to ^{4}He + ^{3}H or ^{8}Be to $2 \times {}^4$He. In this resonance-gas approximation, all known excited states are considered, and states above the threshold energy are assumed to decay and to feed other isotopes in the final distribution.

The second approximation takes the states in the continuum more accurately into account. The virial expansion implements continuum correlations in a systematic way. This virial approximation is also known from the nuclear matter equation of state [26,29,30].

In the third approximation, in-medium modifications are taken into account. These are the shifts of binding energies owing to Pauli blocking and possible dissolution of bound states if they are shifted to the continuum [19,31,32].

A. Excited states and resonance-gas approximation

Data for excited states are shown in the Appendix, Tables IV–VIII. In addition, the threshold energy E_{AZ}^{thresh} is shown for the continuum of scattering states. As indicated above, this is in general the neutron separation energy S_n, but other decay channels (e.g. triton, α) are also possible. For each isotope of the primary distribution, different final states are possible if excited, unstable states are considered. A branching ratio would indicate the ratio to final-state transitions during the expansion after freezeout.

We use the simple approximation that all excited states below the continuum edge decay to the ground state of the same isotope. States above the continuum edge decay to other final isotopes. The same happens also with the unbound nuclei
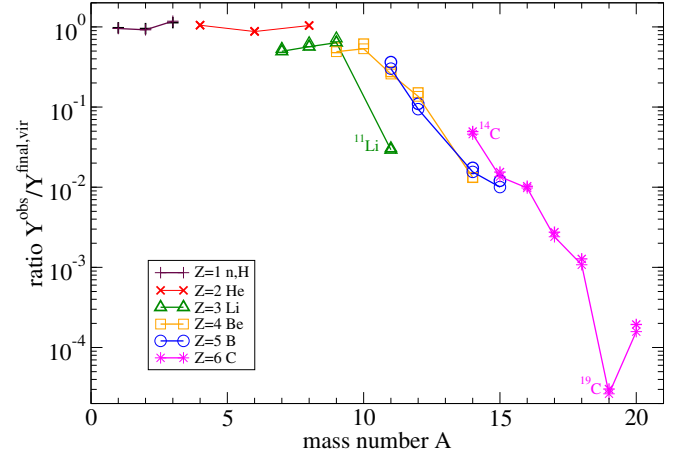
such as ^{4}H, ^{5}He. These states, which feed down to other isotopes, are marked with an asterisk (*), and the process is indicated ($\rightarrow {}^3$H for ^{4}H, etc.). Weakly bound states within 1 MeV below the threshold energy are marked with "0". In the present approximation of the ideal resonance gas, we assume that these states contribute to the ground-state final yield of the same isotope after deexcitation. The corresponding factors $R_{A,Z}^{\text{res.gas}}(\lambda_T)$, which are related to the intrinsic partition function, are calculated for $\lambda_T = 1.29$ MeV in Tables IV–VIII. These partition function multipliers are also shown in Tables I, II, together with the relevant, primary yields $Y_{A,Z}^{\text{rel,res.gas}}$, and the final yields $Y_{A,Z}^{\text{final,res.gas}}$.

To compare with the observed yields, results for the ratio $Y_{A,Z}^{\text{obs}}/Y_{A,Z}^{\text{final,res.gas}}$ for this resonance-gas approximation are shown in Table III as well as in Fig. 3. The global behavior can be described as follows: Up to $A = 10$ the observed yields are rather well reproduced by the grand canonical equilibrium calculations, for larger A we see a strong suppression, as has already been discussed in Refs. [14,18,20]. Individual isotopes show deviations from the global behavior, which may be caused by the approximations in calculating the final distribution, i.e., neglecting interaction effects. This clearly bears further investigation.

B. Virial expansion and continuum correlations

As previously indicated we have improved the equilibrium calculations in two successive steps. First we consider the virial expansion, which accounts for continuum contributions. In the subsequent section, in-medium effects are also taken into account. Results for the virial approximation are shown in Table III and Fig. 3.

The cluster-virial expansion considers continuum correlations of two constituents of nuclear matter in terms of the scattering phase shifts, as obtained in correspondence to the Beth-Uhlenbeck formula. For instance, ^{4}H is considered as resonance in the $t - n$ channel, where scattering phase shifts

TABLE III. Observed yields per fission of ternary fission of ^{241}Pu(n_{th}, f) are compared to a final-state distribution, obtained from feeding of a relevant (primary) distribution. The primary distribution was calculated in the ideal resonance-gas approximation (res.gas), as well as for the virial form (vir) and including medium effects (medium). Lagrange parameters and other properties are given at the bottom of the table, the fit metric refers to all isotopes with $Z \leqslant 2$. Units: MeV for $B_{A,Z}$, E_{AZ}^{thresh}, λ_i, fm^3 for volume, and for n_B fm^{-3}.

isotope	A	Z	$\frac{B_{A,Z}}{A}$	$g_{A,Z}$	E_{AZ}^{thresh}	$Y_{A,Z}^{\text{obs}}$	$Y_{A,Z}^{\text{obs}}/Y_{A,Z}^{\text{final,res.gas}}$	$Y_{A,Z}^{\text{obs}}/Y_{A,Z}^{\text{final,vir}}$	$Y_{A,Z}^{\text{obs}}/Y_{A,Z}^{\text{final,medium}}$
1n	1	0	0	2	–	0.107	0.9742	0.9555	0.9551
1H	1	1	0	2	–	–	–	–	–
2H	2	1	1.112	3	2.224	8.463×10^{-6}	0.952	0.92	0.917
3H	3	1	2.827	2	6.257	1.584×10^{-4}	1.133	1.179	1.223
4He	4	2	7.073	1	20.577	2.015×10^{-3}	1.055	1.049	1.042
6He	6	2	4.878	1	0.975	5.239×10^{-5}	0.8856	0.8753	0.8903
8He	8	2	3.925	1	2.125	3.022×10^{-6}	1.043	1.04	1.03
7Li	7	3	5.606	4	2.461	1.35×10^{-6}	0.5305	0.4964	0.4523
8Li	8	3	5.160	5	2.038	8.463×10^{-7}	0.6235	0.5669	0.5211
9Li	9	3	5.038	4	4.062	1.672×10^{-6}	0.7164	0.6363	0.5814
11Li	11	3	4.155	4	0.396	9.068×10^{-10}	0.03061	0.02936	0.2992
9Be	9	4	6.462	4	1.558	8.866×10^{-7}	0.5488	0.4908	0.3191
10Be	10	4	6.497	1	6.497	9.269×10^{-6}	0.6149	0.5343	0.5285
11Be	11	4	5.953	2	0.502	1.189×10^{-6}	0.2756	0.2584	0.4202
12Be	12	4	5.721	1	3.17	5.642×10^{-7}	0.1513	0.1362	0.1385
14Be	14	4	4.994	1	1.264	5.441×10^{-10}	0.01321	0.01326	0.0121
11B	11	5	6.928	4	8.674	3.224×10^{-7}	0.3632	0.3015	0.2257
12B	12	5	6.631	3	3.369	2.015×10^{-7}	0.1098	0.09418	0.08358
14B	14	5	6.102	5	0.97	2.62×10^{-8}	0.01742	0.01552	0.01793
15B	15	5	5.880	4	2.78	9.269×10^{-9}	0.01205	0.01005	0.008624
14C	14	6	7.520	1	8.176	2.539×10^{-6}	0.0495	0.04598	0.02229
15C	15	6	7.100	2	1.218	8.665×10^{-7}	0.01546	0.01353	0.01464
16C	16	6	6.922	1	4.25	1.008×10^{-6}	0.01028	0.009781	0.007721
17C	17	6	6.558	4	0.734	1.29×10^{-7}	0.002748	0.00241	0.005271
18C	18	6	6.426	1	4.18	5.642×10^{-8}	0.001276	0.001078	0.0006891
19C	19	6	6.118	2	0.58	5.038×10^{-10}	0.00003031	0.00002647	0.0002309
20C	20	6	5.961	1	2.98	7.254×10^{-10}	0.0001937	0.0001578	0.0001285
λ_T	–	–	–	–	–	–	1.2897	1.2913	1.2924
λ_n	–	–	–	–	–	–	−3.1486	−3.1425	−3.087
λ_p	–	–	–	–	–	–	−16.273	−16.236	−16.189
volume	–	–	–	–	–	–	1859.4	1876.4	1796.3
n_B	–	–	–	–	–	–	0.000064	0.0000645	0.00006741
Y_p	–	–	–	–	–	–	0.03486	0.03486	0.03479
fit metric	–	–	–	–	–	–	0.005485	0.009384	0.009574

have been measured, see Refs. [19,30]. For details see the Appendix C. Data for $R_{A,Z}^{\text{vir}}(T)$ are shown in the Appendix, Tables IV–VIII. The resulting ratios $Y_{A,Z}^{\text{obs}}/Y_{A,Z}^{\text{final,vir}}$ are also shown in Table III.

We see that the changes are small in general, so that the influence of the continuum correlations on the final yield distribution is not essential. This may be attributed to the low temperature so that the contribution of scattering states is small for binding energies larger than T. At higher T, the contribution of scattering states would become more important. As shown by the partition function multipliers given in Table IV in Appendix A, the most important changes are obtained for ^{4}H so that the feed down to the final ^{3}H is reduced. Some He isotopes are also reduced. The optimum fit of Lagrange parameters is also slightly changed. However, for several of the isotopes considered, strong deviations from the global behavior remain.

As discussed in the case of ^{6}He [20], weakly bound states are more sensitive to medium effects. The threshold energy of ^{11}Li is low, and the yield is strongly overestimated within the ideal gas and virial approaches. Obviously, the measured yield of ^{11}Li is not well described in the approximations where the interaction between the components is neglected.

Low yields of other exotic nuclei (^{19}C, etc.) are also known, and are observed in ternary fission of other actinides (Am, Cf, etc.). For the carbon isotopes, the spectrum of excited states is rather complex and feeds different final states. In particular, isotopes with excited states above the neutron separation energy feed the yield of isotopes with $A - 1$. Calculations of the yields, see Figs. 3 and 4 in Ref. [37], cannot explain the low yield for ^{19}C. As seen there, the authors offer no explanation for the low yield of these exotic neutron-rich, halolike nuclei.

TABLE IV. Data of nucleons/nuclei $Z \leqslant 2$ [units: MeV for $B_{A,Z}$, E_{AZ}^{thresh}, E_i]. Feed down to other final isotopes indicated by $\rightarrow^A Z$. Mass number A, charge number Z. Ground-state binding energy $B_{A,Z}$ and degeneracy $g_{A,Z} = 2J + 1$, continuum threshold energy E_{AZ}^{thresh}, excitation energy E_i, and degeneracy g_i according to Ref. [33]. Partition function multiplier $R_{A,Z}^{\text{res.gas}}(T)$ according to (C5). The contribution of excited states above the continuum threshold is denoted by "*", the contribution of states within 1 MeV below the threshold is denoted by "0" (weakly bound states).

isotope	feed down	A	Z	$B_{A,Z}/A$	$g_{A,Z}$	E_{AZ}^{thresh}	E_i [g_i]	$R_{A,Z}^{\text{res.gas}}(1.29)$	$R_{A,Z}^{\text{vir}}(1.29)$	$R_{A,Z}^{\text{medium}}(1.29)$
^{1}n	–	1	0	0	2	–	–	1	1	1
^{1}H	–	1	1	0	2	–	–	1	1	1
^{2}H	–	2	1	1.112	3	2.224	–	1	0.974	0.9306
^{3}H	–	3	1	2.827	2	6.257	–	1	0.999	0.9138
^{4}H*	$\rightarrow ^3$H	4	1	1.720	5	−1.6	0.31 [3], 2.08 [1], 2.83 [3]	1.579	0.09404	0.03564
^{3}He	–	3	2	2.573	2	5.494	–	1	0.9979	0.9545
^{4}He	–	4	2	7.073	1	20.577	20.21 [1]	1	1	0.915
^{5}He*	$\rightarrow ^4$He	5	2	5.512	4	−0.735	–	1	0.6906	0.5029
^{6}He^0	[$\rightarrow ^4$He]	6	2	4.878	1	0.975	–	1	0.9343	0.7723
^{6}He*	$\rightarrow ^4$He	6	2	4.878	1	0.975	1.797 [5]	1.242	0.7919	0.4617
^{7}He*	$\rightarrow ^6$He	7	2	4.123	4	−0.410	2.92 [6]	1.156	0.9313	0.6577
^{8}He	–	8	2	3.925	1	2.125	–	1	0.972	0.7383
^{8}He*	$\rightarrow ^4$He	8	2	3.925	1	2.125	3.1 [5]	0.452	0.2334	0.06923
^{9}He*	$\rightarrow ^8$He	9	2	3.349	2	−1.25	1.1 [2]	1.426	0.364	0.04882

TABLE V. Data of lithium nuclei [units: MeV for $B_{A,Z}$, E_{AZ}^{thresh}, E_i]. Feed down to other final isotopes indicated by $\rightarrow^A Z$. Mass number A, charge number Z. Ground-state binding energy $B_{A,Z}$ and degeneracy $g_{A,Z} = 2J + 1$, continuum threshold energy E_{AZ}^{thresh}, excitation energy E_i, and degeneracy g_i according to Ref. [33]. Partition function multiplier $R_{A,Z}^{\text{res.gas}}(T)$ according to (C5) for $\lambda_T = 1.29$ MeV. ^{7}Li: E_{AZ}^{thresh} for decay to ^{4}He $+ ^3$H; excited states at 4.630 MeV [8], 6.680 MeV [6] decay this way, but also γ decay.

isotope	feed down	A	Z	$B_{A,Z}/A$	$g_{A,Z}$	E_{AZ}^{thresh}	E_i [g_i]	$R_{A,Z}^{\text{res.gas}}(1.29)$	$R_{A,Z}^{\text{vir}}(1.29)$	$R_{A,Z}^{\text{medium}}(1.29)$
6Li	–	6	3	5.332	3	1.475	–	1	0.9544	0.83
6Li*	$\rightarrow ^3$H	6	3	5.332	3	1.475	2.186 [7], 3.563 [1], 4.312 [5], 5.366 [5], 5.65 [3]	0.5471	0.3847	0.2842
7Li	–	7	3	5.606	4	2.461	0.478 [2]	1.345	1.316	1.097
8Li	–	8	3	5.160	5	2.038	0.980 [3]	1.281	1.242	0.9877
8Li*	$\rightarrow ^7$Li	8	3	5.160	(5)	2.038	2.255 [7], 3.210 [3], 5.4 [3], 6.1 [7]	0.3151	0.2646	0.1975
9Li	–	9	3	5.038	4	4.062	2.691 [2], (4.301) [?]	1.062	1.055	0.8069
10Li*	$\rightarrow ^9$Li	10	3	4.531	(3)	−0.032	–	1	0.863	0.5866
11Li^0	[$\rightarrow ^9$Li]	11	3	4.155	4	0.396	(1.266) [?]	1	0.9003	0.6026
12Li*	$\rightarrow ^{11}$Li	12	3	3.792	(3)	−0.201	–	1	0.8422	0.4697

TABLE VI. Data of beryllium nuclei [units: MeV for $B_{A,Z}$, E_{AZ}^{thresh}, E_i]. Feed down to other final isotopes indicated by $\rightarrow^A Z$. Mass number A, charge number Z. Ground-state binding energy $B_{A,Z}$ and degeneracy $g_{A,Z} = 2J + 1$, continuum threshold energy E_{AZ}^{thresh}, excitation energy E_i, and degeneracy g_i according to Ref. [33]. Partition function multiplier $R_{A,Z}^{\text{res.gas}}(T)$ according to (C5) for $\lambda_T = 1.29$ MeV. Weakly bound isotopes ^{10}Be^0, ^{11}Be^0, and ^{12}Be^0 are separated, they will merge with the continuum at higher densities.

isotope	feed down	A	Z	$B_{A,Z}/A$	$g_{A,Z}$	E_{AZ}^{thresh}	E_i [g_i]	$R_{A,Z}^{\text{res.gas}}(1.29)$	$R_{A,Z}^{\text{vir}}(1.29)$	$R_{A,Z}^{\text{medium}}(1.29)$
7Be	–	7	4	5.372	4	1.585	0.429 [2]	1.359	1.302	1.1324
8Be*	$\rightarrow ^4$He	8	4	7.062	1	−0.088	3.03 [5]	1.477	1.266	1.0192
9Be	–	9	4	6.462	4	1.558	–	1	0.9572	0.7585
9Be*	$\rightarrow ^4$He	9	4	6.462	(4)	1.558	1.684 [2], 2.429 [6], 2.78 [2], 3.049 [6]	0.5628	0.4796	0.3629
10Be	–	10	4	6.497	1	6.497	3.368 [5]	1.367	1.366	1.0462
10Be^0	[$\rightarrow ^9$Be]	10	4	6.497	(1)	6.497	5.958 [5], 5.959 [3]	0.0789	0.07181	0.05348
11Be^0	[$\rightarrow ^{10}$Be]	11	4	5.953	2	0.502	–	1	0.9076	0.6422
11Be^0	[$\rightarrow ^{10}$Be]	11	4	5.953	(2)	0.502	0.320 [2]	0.7803	0.6894	0.4802
11Be*	$\rightarrow ^{10}$Be	11	4	5.953	(2)	0.502	1.783 [6], 2.654 [4], 3.4 [4], 3.889 [4], 3.955 [4]	1.343	0.308	0.03957
12Be	–	12	4	5.721	1	3.170	2.109 [5], 2.251 [1]	2.149	2.122	1.4798
12Be^0	[$\rightarrow ^{10}$Be]	12	4	5.721	(1)	3.170	2.715 [3]	0.3657	0.3307	0.222
13Be*	$\rightarrow ^{12}$Be	13	4	5.241	2	−0.510	–	1	0.7806	0.3144
14Be	–	14	4	4.994	1	1.264	–	1	0.9468	0.5897
15Be*	$\rightarrow ^{14}$Be	15	4	4.541	6	−1.800	–	1	0.02241	0.0005243

TABLE VII. Data of boron nuclei [units: MeV for $B_{A,Z}$, E_{AZ}^{thresh}, E_i]. Feed down to other final isotopes indicated by $\rightarrow^A Z$. Mass number A, charge number Z. Ground-state binding energy $B_{A,Z}$ and degeneracy $g_{A,Z} = 2J + 1$, continuum threshold energy E_{AZ}^{thresh}, excitation energy E_i and degeneracy g_i according to Ref. [33]. Partition function multiplier $R_{A,Z}^{\text{res.gas}}(T)$ according to (C5) for $\lambda_T = 1.29$ MeV.

isotope	feed down	A	Z	$B_{A,Z}/A$	$g_{A,Z}$	E_{AZ}^{thresh}	$E_i\ [g_i]$	$R_{A,Z}^{\text{res.gas}}(1.29)$	$R_{A,Z}^{\text{vir}}(1.29)$	$R_{A,Z}^{\text{medium}}(1.29)$
10B	–	10	5	6.475	7	4.466	0.718 [3], 1.740 [1], 2.154 [3]	1.363	1.357	1.086
$10B^0$	–	10	5	6.475	(7)	4.466	3.587 [5]	0.0443	0.04117	0.0324
11B	–	11	5	6.928	4	8.674	2.124 [2], 4.445 [6], 5.020 [4], 6.741 [8]	1.175	1.175	0.9
12B	–	12	5	6.631	3	3.369	0.953 [5], 1.674 [5]	2.251	2.227	1.626
$12B^0$	[$\rightarrow ^{11}$B]	12	5	6.631	3	3.369	2.621 [3], 2.723 [1]	0.1715	0.1582	0.1127
13B	–	13	5	6.496	4	4.879	3.482 [?], 3.535 [?], 3.681 [?], 3.712 [?], 4.131 [?]	1	0.9966	0.6976
$14B^0$	–	14	5	6.102	5	0.970	–	1	0.9341	0.6065
$14B^0$	[$\rightarrow ^{13}$B]	14	5	6.102	(5)	0.970	0.740 [3]	0.3381	0.3001	0.188
$14B^*$	$\rightarrow ^{13}$B	14	5	6.102	(5)	0.970	1.38 [7]	0.4803	0.387	0.1801
15B	–	15	5	5.880	4	2.78	(?)	1	0.983	0.6246
$16B^*$	$\rightarrow ^{15}$B	16	5	5.507	1	−0.082	(?)	1	0.8574	0.4311
17B	–	17	5	5.270	4	1.39	(?)	1	0.9515	0.5399
$18B^*$	$\rightarrow ^{17}$B	18	5	4.977	5	−0.005	(?)	1	0.8659	0.3832

C. In-medium effects

We now consider two medium effects, which might modify the yield distributions: self-energy shifts and Pauli blocking. Self-energy shifts act on all nucleons and can be accounted for by a renormalization of the chemical potentials $\tilde{\lambda}_n$, $\tilde{\lambda}_p$ if they are not momentum dependent. Ratios of yields are not influenced by these shifts. In contrast, Pauli blocking acts individually for each isotope and leads to strong deviations of the yield distribution.

Self-energy of nucleons has been treated, for instance, within the relativistic mean-field approximation. The well-established parametrization of DD2-RMF [38] gives for the parameter values $T = 1.29$ MeV, $n_B = 0.000067$ fm^{-3}, $Y_p = 0.035$ the self-energy shifts $\Delta_n^{\text{SE}} = -0.03934$ MeV, $\Delta_p^{\text{SE}} = -0.09936$ MeV. For a cluster $\{A, Z\}$ the self-energy shift is $\Delta E_{A,Z}^{\text{SE}} = (A - Z)\Delta_n^{\text{SE}} + Z\Delta_p^{\text{SE}}$. We then have $\tilde{\lambda}_n = \lambda_n - \Delta_n^{\text{SE}}$, $\tilde{\lambda}_p = \lambda_p - \Delta_p^{\text{SE}}$.

In all our earlier fits [20], the yields of ^{6}He are overestimated, whereas the yields of ^{8}He are underestimated. One possible explanation is that ^{6}He is only weakly bound ($E^{\text{thresh}} = 0.975$ MeV) compared to ^{8}He ($E^{\text{thresh}} = 2.125$ MeV). In the dense medium, binding energies are shifted, and weakly bound states are more affected than strongly bound states.

More visible in Fig. 3 is the strong suppression of weakly bound isotopes such as ^{11}Li and ^{19}C. These isotopes are near to the continuum edge so that the shift owing to Pauli blocking may lead to dissolution (the Mott effect [26]). This suggests the use of yields of weakly bound states as test probes to infer the free neutron density. The observation of such Mott effects would provide us with an independent test of the free neutron density at scission.

To quantify this effect, we consider the bound-state contribution to the intrinsic partition function, which contains the

TABLE VIII. Data of carbon nuclei [units: MeV for $B_{A,Z}$, E_{AZ}^{thresh}, E_i]. Feed down to other final isotopes indicated by $\rightarrow^A Z$. Mass number A, charge number Z. Ground-state binding energy $B_{A,Z}$ and degeneracy $g_{A,Z} = 2J + 1$, continuum threshold energy E_{AZ}^{thresh}, excitation energy E_i, and degeneracy g_i according to Ref. [33]. Partition function multiplier $R_{A,Z}^{\text{res.gas}}(T)$ according to (C5) for $\lambda_T = 1.29$ MeV.

| isotope	feed down	A	Z	$B_{A,Z}/A$	$g_{A,Z}$	E_{AZ}^{thresh}	$E_i\ [g_i]$	$R_{A,Z}^{\text{res.gas}}(1.29)$	$R_{A,Z}^{\text{vir}}(1.29)$	$R_{A,Z}^{\text{medium}}(1.29)$
13C	–	13	6	7.469	2	4.946	3.089 [2], 3.684 [4], 3.853[6]	1.358	1.353	0.9905
14C	–	14	6	7.520	1	8.176	6.093 [3], 6.589 [7]	1.069	1.069	0.7491
15C	–	15	6	7.100	2	1.218	–	1	0.945	0.6169
$15C^0$	[$\rightarrow ^{14}$C]	15	6	7.100	(2)	1.218	0.740 [6]	1.69	1.532	0.9775
$15C^*$	$\rightarrow ^{14}$C	15	6	7.100	(2)	1.218	3.103 [2], 4.220 [6], 4.657 [4], 4.780 [4]	0.3074	0.004482	0.000206
16C	–	16	6	6.922	1	4.250	1.766 [5]	2.272	2.26	1.445
$16C^0$	[$\rightarrow ^{15}$C]	16	6	6.922	(1)	4.250	3.986 [5], 4.089 [7], 4.142 [9]	0.885	0.7875	0.4683
$17C^0$	[$\rightarrow ^{16}$C]	17	6	6.558	4	0.734	–	1	0.9218	0.5379
$17C^0$	[$\rightarrow ^{16}$C]	17	6	6.558	(4)	0.734	0.217 [2], 0.332 [6]	1.582	1.438	0.8288
$17C^*$	$\rightarrow ^{16}$C	17	6	6.558	(4)	0.734	2.15 [8], 2.71 [2], 3.085 [10]	0.6677	0.09067	0.002612
18C	–	18	6	6.426	1	4.18	1.588 [5], 2.515 [5]	3.172	3.153	1.843
$19C^0$	[$\rightarrow ^{18}$C]	19	6	6.118	2	0.580	0.209 [4], 0.282 [6]	5.112	4.665	2.431
$19C^*$	$\rightarrow ^{18}$C	19	6	6.118	(2)	0.580	0.653 [6], 1.46 [6]	2.776	2.383	0.9985
20C	–	20	6	5.961	1	2.98	1.618 [5]	2.426	2.391	1.268
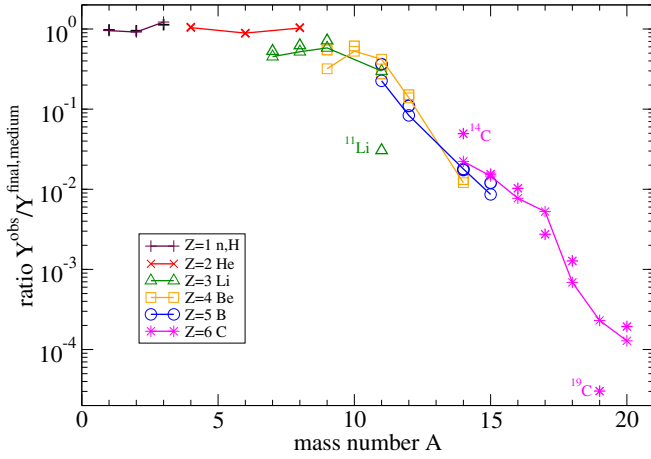
FIG. 4. Ternary fission of ^{241}Pu(n_{th}, f): Ratios $Y_{A,Z}^{\text{obs}}/Y_{A,Z}^{\text{final,res.gas}}$ (bold symbols) and $Y_{A,Z}^{\text{obs}}/Y_{A,Z}^{\text{final,medium}}$ (full lines) as function of the mass number A. Isotopes with $Z \leqslant 6$ are shown. Data from Tables III, IX, X.

factor $e^{-E_{A,Z}^0/T} - 1$ [18]. If the bound-state energy is shifted owing to in-medium effects, this factor is also changed and goes to zero at the Mott density where bound states disappear.

The Pauli blocking shift of bound states in dense matter and the Mott effect has previously been considered in detail for individual isotopes [19,26,31]. We will give here only a general estimate applicable to bound states of all nuclei. The shift of bound-state energies $E_{A,Z}(T, n_B, Y_p) - E_{A,Z}^0$ in a dense medium (Pauli blocking) has been estimated in Ref. [19], Eq. (22), for nucleons in the $1s$ and $1p$ orbits as

$$\Delta E_{A,Z}^{\text{Pauli}} = 1064(A - Z)n_B e^{-0.0513\,T/[\text{MeV}]}\text{MeV fm}^3, \quad (4)$$

where we assume that the proton contribution is negligible because of its very low density. With the baryon density $n_B = 6.7 \times 10^{-5}$ fm^{-3} (which should be determined self-consistently), the shifts of the binding energy of the different isotopes are given in Tables IX and X. These shifts may become important for weakly bound states. For instance, for ^{11}Li the shift is larger than the threshold energy so that the bound state is dissolved. This is also reflected in the low observed yield of this isotope. In a more detailed calculation [39] not considered here, the Pauli blocking shift depends on the center-of-mass momentum P of the cluster. Because the shift becomes smaller for larger total momentum P, and continuum correlations may be present, a small yield of this isotope remains. The same happens also with ^{19}C where the shift is also larger than the threshold energy so that the Mott effect leads to a significant reduction of the observed yields. This is also seen in Fig. 4. The yields of other isotopes with a low threshold energy ($E_{AZ}^{\text{thresh}} < 1$ MeV) will be significantly influenced too. The excited states ^{11}Be^0, ^{14}B^0, ^{15}C$^0 - ^{17}$C^0 become dissolved because of Pauli blocking. The corresponding calculations are seen in Tables IX, X.

As shown from Table III and Fig. 4, the observed yields are, in fact, sensitive to in-medium effects. Suppression effects owing to Pauli blocking seem to be visible. This allows an independent second determination of the baryon density, and

the densities at which such isotopes, which are dissolved, are consistent with the inferred value $n_B = 6.7 \times 10^{-5}$ fm^{-3}. Note that a fully *ab initio* calculation of the Pauli blocking effects is very involved, and we gave here only exploratory calculations to illustrate the effect of suppression.

V. GENERALIZED RELATIVISTIC MEAN-FIELD APPROACH

As discussed above, important in-medium effects are self-energy shifts and Pauli blocking. If the self-energy shifts are not dependent on the nucleon momentum, they can be absorbed into the chemical potential thus creating an effective chemical potential. Different approximations may be used to describe the in-medium self-energy shifts, for instance, the Skyrme or the relativistic mean-field approaches.

In Ref. [40], Pais *et al.* reported a generalized relativistic mean-field (RMF) approach formulated for the study of in-medium modifications on light cluster properties. Explicit binding energy shifts and a modification of the scalar cluster-meson coupling were introduced in order to take these medium effects into account. The interactions of the clusters $i = {^2}$H, ^{3}H, ^{3}He, ^{4}He with the surrounding medium are described with a phenomenological modification, x_s, of the coupling constant to the σ meson, $g_{\sigma_i} = x_s A_i g_\sigma$, where g_σ is the nucleon scalar coupling, and A_i the number of nucleons in cluster i.

Using the FSU Gold EoS [41], and requiring that the cluster fractions exhibit the correct behavior in the low-density virial limit [42,43], they obtained a universal scalar cluster-meson coupling fraction, $x_{\sigma_i} = 0.85 \pm 0.05$, which could reproduce both this limit and the equilibrium constants extracted from reaction ion data [44] reasonably well. We note that the vector cluster-meson coupling is defined as $g_{v_j} = A_j g_v$. Later this work was generalized to include clusters up to $A = 12$ [45]. A recent analysis of the deuteron-meson coupling at zero temperature was presented by Burrello and Typel [46], and suitable parameterizations of the cluster mass shift at zero temperature were derived for all baryon densities.

In the present paper, we keep the same model as in Ref. [40], the FSU Gold EoS [41], instead of the model used in the previous section, the DD2 EoS [38], but we note that both parametrizations yield approximately the same values for the quasiparticle energy shifts at the very low densities considered here. However, under such dilute-matter conditions, other models may be more suitable [47,48].

In a more recent work [49], Pais *et al.* compared results of an analysis, where in-medium effects are included, to experimental equilibrium constants measured in intermediate energy Xe + Sn collisions. This comparison required a higher scalar cluster-meson coupling constant $x_s = 0.92 \pm 0.02$. With this higher assumed value of the coupling constant, the in-medium effects are reduced, and the clusters melt at larger densities.

In the top panel of Fig. 5, we show the mass fractions of the clusters with $Z = 1, 2$ and also the fraction of the free neutron gas, calculated using the RMF formalism with $x_s = 0.85$, as a function of the density for the temperature and proton fraction found in the QS approach with in-medium effects described in

TABLE IX. Calculated yields per fission of ternary fission of ^{241}Pu(n_{th}, f), in-medium effects included. For the fit of the ^{241}Pu(n_{th}, f) data, the Lagrange parameter values are $\lambda_T = 1.29$, $\tilde{\lambda}_n = -3.09$, $\tilde{\lambda}_p = -16.19$ MeV, volume 1796 fm^3, fit metric 0.0095 for all nuclei $Z \leqslant 2$. Baryon density $n_B = 6.7 \times 10^{-5}$, $Y_p = 0.035$. Bold figures: Mott effect, the Pauli blocking shift exceeds the ground state binding energy so that the bound state is dissolved. For illustration of this effect, a branching ratio 0.1 is assumed to remain as final yield (denoted by superscript "+") whereas 0.9 is assumed to feed down the yields of other isotopes. [Units: MeV for $B_{A,Z}$, E^{thresh}_{AZ}, $\Delta E^{\text{Pauli}}_{A,Z}$].

isotope	A	Z	$\frac{B_{A,Z}}{A}$	$g_{A,Z}$	E^{thresh}_{AZ}	$R^{\text{vir}}_{A,Z}(1.29)$	$\Delta E^{\text{Pauli}}_{A,Z}$	$R^{\text{medium}}_{A,Z}(1.29)$	$Y^{\text{rel,medium}}_{A,Z}$	$Y^{\text{final,medium}}_{A,Z}$	$Y^{\text{obs}}_{A,Z}/Y^{\text{final,medium}}_{A,Z}$
1n	1	0	0	2	–	1	–	1	0.11203	0.11203	0.9551
1H	1	1	0	2	–	1	–	1	4.563×10^{-6}	4.563×10^{-6}	–
2H	2	1	1.112	3	2.224	0.9739	0.057	0.9306	9.226×10^{-6}	9.226×10^{-6}	0.9173
3H	3	1	2.827	2	6.257	0.9988	0.114	0.9138	1.289×10^{-4}	1.342×10^{-4}	1.223
4H*	4	1	1.720	5	−1.6	0.09404	0.172	0.03564	5.146×10^{-6}	[$\to$ ^{3}H]	–
3He	3	2	2.573	2	5.494	0.9979	0.057	0.9545	2.948×10^{-9}	2.948×10^{-9}	–
4He	4	2	7.073	1	20.577	1	0.114	0.915	1.639×10^{-3}	1.935×10^{-3}	1.042
5He*	5	2	5.512	4	−0.735	0.6906	0.172	0.5029	2.622×10^{-4}	[$\to$ ^{4}He]	–
6He^0	6	2	4.878	1	0.975	0.9343	0.2291	0.7723	4.575×10^{-5}	5.884×10^{-5}	0.8903
6He*	6	2	4.878	1	0.975	0.7919	0.2291	0.4617	2.735×10^{-5}	[$\to$ ^{4}He]	–
7He*	7	2	4.123	4	−0.410	0.9313	0.2864	0.6577	1.309×10^{-5}	[$\to$ ^{6}He]	–
8He	8	2	3.925	1	2.125	0.972	0.3437	0.7383	2.919×10^{-6}	2.935×10^{-6}	1.029
8He*	8	2	3.925	1	2.125	0.2332	0.3437	0.06923	2.737×10^{-7}	[$\to$ ^{4}He]	–
9He*	9	2	3.349	2	−1.25	0.364	0.4009	0.04882	1.605×10^{-8}	[$\to$ ^{8}He]	–
6Li	6	3	5.332	3	1.475	0.9545	0.172	0.83	4.78×10^{-8}	4.78×10^{-8}	–
6Li*	6	3	5.332	3	1.475	0.3847	0.172	0.2842	1.417×10^{-8}	[$\to$ ^{3}H]	–
7Li	7	3	5.606	4	2.461	1.3159	0.2291	1.0972	2.66×10^{-6}	2.985×10^{-6}	0.4523
8Li	8	3	5.160	5	2.038	1.2424	0.2864	0.9877	1.624×10^{-6}	1.624×10^{-6}	0.5211
8Li*	8	3	5.160	(5)	2.038	0.2647	0.2864	0.1975	3.247×10^{-7}	[$\to$ ^{7}Li]	–
9Li	9	3	5.038	4	4.062	1.0553	0.3437	0.8069	2.694×10^{-6}	2.876×10^{-6}	0.5814
10Li*	10	3	4.531	*3*	−0.032	0.863	0.4009	0.5866	1.539×10^{-7}	[$\to$ ^{9}Li]	–
11Li$^+$	11	3	4.155	4	**0.396**	0.9003	**0.4582**	0.6026	$3.03 \times 10^{-8} \times 0.1$	3.03×10^{-9}	0.2992
11Li^0	11	3	4.155	4	**0.396**	0.9003	**0.4582**	0.6026	$3.03 \times 10^{-8} \times 0.9$	[$\to$ ^{9}Li]	–
12Li*	12	3	3.792	*3*	−0.201	0.8422	0.5155	0.4697	1.585×10^{-9}	[$\to$ ^{9}Li]	–
7Be	7	4	5.372	4	1.585	1.3015	0.172	1.1324	3.058×10^{-11}	3.058×10^{-11}	–
8Be*	8	4	7.062	1	−0.088	1.2657	0.2291	1.0192	1.722×10^{-6}	[$\to$ ^{4}He]	–
9Be	9	4	6.462	4	1.558	0.9572	0.2864	0.7585	2.03×10^{-6}	2.778×10^{-6}	0.3191
9Be*	9	4	6.462	4	1.558	0.4796	0.2864	0.3629	9.712×10^{-7}	[$\to$ ^{4}He]	–
10Be	10	4	6.497	1	6.497	1.366	0.3437	1.0462	1.464×10^{-5}	1.752×10^{-5}	0.5285
10Be^0	10	4	6.497	(1)	6.497	0.07181	0.3437	0.05348	7.482×10^{-7}	[$\to$ ^{9}Be]	–
11Be	11	4	5.953	2	0.502	0.9076	0.4009	0.6422	2.829×10^{-6}	2.829×10^{-6}	0.4202
11Be^0	11	4	5.953	2	0.502	0.6894	0.4009	0.48015	1.141×10^{-6}	[$\to$ ^{10}Be]	–
11Be*	11	4	5.953	(2)	0.502	0.308	0.4009	0.03957	3.341×10^{-9}	[$\to$ ^{10}Be]	–
12Be	12	4	5.721	1	3.170	2.1223	0.4582	1.4798	3.957×10^{-6}	4.074×10^{-6}	0.1385
12Be^0	12	4	5.721	(1)	3.170	0.3307	0.4582	0.222	5.937×10^{-7}	[$\to$ ^{10}Be]	–
13Be*	13	4	5.241	2	−0.510	0.7806	0.5155	0.3144	1.164×10^{-7}	[$\to$ ^{12}Be]	–
14Be	14	4	4.994	1	1.264	0.9468	0.5728	0.5897	4.497×10^{-8}	4.498×10^{-8}	0.01209
15Be*	15	4	4.541	6	−1.800	0.02241	0.6301	0.0005243	5.994×10^{-12}	[$\to$ ^{14}Be]	–

the previous section. In the bottom panel, the mass fractions of light particles are plotted against the density, for different values of the scalar cluster-meson coupling. We observe that the abundances shown in the top panel are quite similar to the ones in the resonance-gas approximation (see Fig. 1). Also, from the bottom panel, we see that the medium effects are almost negligible because the densities are very small. As it was shown in Table III, the effect of the medium is more relevant when considering clusters with higher Z.

In Fig. 6, we present the calculated fit metrics derived with different values of the scalar cluster-meson coupling constant, and we observe a minimum at about the same density as in the QS approach, $n_B \sim 6.7 \times 10^{-5}$ fm^{-3}.

VI. CONCLUSIONS

We have considered the modeling of ternary fission yields within a systematic quantum statistical approach and a generalized relativistic mean-field approach. We consider our quantum statistical approach as a first step in a strict nonequilibrium approach. As an example, we have analyzed the observed yields for ^{241}Pu(n_{th}, f).

We assume that the light charged fragments are emitted from the neck region at scission. We have first considered partial chemical equilibrium for clusters $Z \leqslant 2$. During the further expansion, feed-down processes were considered. This leads to the final yields, which are compared to the observed

TABLE X. Continuation of Table IX.

isotope	A	Z	$\frac{B_{A,Z}}{A}$	$g_{A,Z}$	E_{AZ}^{thresh}	$R_{A,Z}^{\text{vir}}(1.29)$	$\Delta E_{A,Z}^{\text{Pauli}}$	$R_{A,Z}^{\text{medium}}(1.29)$	$Y_{A,Z}^{\text{rel,medium}}$	$Y_{A,Z}^{\text{final,medium}}$	$Y_{A,Z}^{\text{obs}}/Y_{A,Z}^{\text{final,medium}}$
10B	10	5	6.475	7	4.466	1.357	0.2864	1.086	3.547×10^{-9}	3.547×10^{-9}	–
11B	11	5	6.928	4	8.674	1.175	0.3437	0.9	1.261×10^{-6}	1.428×10^{-6}	0.2258
12B	12	5	6.631	3	3.369	2.227	0.4009	1.626	2.411×10^{-6}	2.411×10^{-6}	0.08358
12B^0	12	5	6.631	(3)	3.369	0.1582	0.4009	0.1127	1.671×10^{-7}	$[\rightarrow {}^{11}\text{B}]$	–
13B	13	5	6.496	4	4.879	0.9966	0.4582	0.6976	6.209×10^{-6}	7.096×10^{-6}	–
14B	14	5	6.102	5	0.970	0.9341	0.5155	0.6065	1.461×10^{-6}	1.461×10^{-6}	0.01793
14B^0	14	5	6.102	(5)	0.970	0.3001	0.5155	0.188	4.53×10^{-7}	$[\rightarrow {}^{13}\text{B}]$	–
14B*	14	5	6.102	(5)	0.970	0.387	0.5155	0.1801	4.338×10^{-7}	$[\rightarrow {}^{13}\text{B}]$	–
15B	15	5	5.880	4	2.78	0.9829	0.5728	0.6246	1.058×10^{-6}	1.075×10^{-6}	0.008624
16B*	16	5	5.507	1	−0.082	0.8574	0.6301	0.4311	1.723×10^{-8}	$[\rightarrow {}^{15}\text{B}]$	–
17B	17	5	5.270	4	1.39	0.9515	0.6873	0.5399	2.723×10^{-8}	2.964×10^{-8}	–
18B*	18	5	4.977	5	−0.005	0.8659	0.7446	0.3832	2.407×10^{-9}	$[\rightarrow {}^{17}\text{B}]$	–
13C	13	6	7.470	2	4.946	1.353	0.4009	0.9905	3.134×10^{-6}	3.137×10^{-6}	–
14C	14	6	7.520	1	8.176	1.069	0.4582	0.7491	6.769×10^{-5}	1.139×10^{-4}	0.02229
15C	15	6	7.100	2	1.218	0.9449	0.5155	0.6169	2.916×10^{-5}	5.92×10^{-5}	0.01464
15C^0	15	6	7.100	(2)	1.218	1.5315	0.5155	0.9775	4.621×10^{-5}	$[\rightarrow {}^{14}\text{C}]$	–
15C*	15	6	7.100	(2)	1.218	0.004482	0.5155	0.000206	9.728×10^{-9}	$[\rightarrow {}^{14}\text{C}]$	–
16C	16	6	6.922	1	4.250	2.259	0.5728	1.445	9.266×10^{-5}	1.305×10^{-4}	0.007721
16C^0	16	6	6.922	(1)	4.250	0.7875	0.5728	0.4683	3.004×10^{-5}	$[\rightarrow {}^{15}\text{C}]$	–
17C	17	6	6.558	4	0.734	0.9218	0.6301	0.5379	2.447×10^{-5}	2.447×10^{-5}	0.005271
17C^0	17	6	6.558	(4)	0.734	1.438	0.6301	0.8288	3.77×10^{-5}	$[\rightarrow {}^{16}\text{C}]$	–
17C*	17	6	6.558	(4)	0.734	0.09067	0.6301	0.002612	1.188×10^{-7}	$[\rightarrow {}^{16}\text{C}]$	–
18C	18	6	6.426	1	4.18	3.153	0.6873	1.843	5.329×10^{-5}	8.188×10^{-5}	0.0006891
19C$^+$	19	6	6.118	2	**0.580**	4.665	**0.7446**	2.431	$2.181 \times 10^{-5} \times 0.1$	2.181×10^{-6}	0.0002309
19C^0	19	6	6.118	2	**0.580**	4.665	**0.7446**	2.431	$2.181 \times 10^{-5} \times 0.9$	$[\rightarrow {}^{18}\text{C}]$	–
19C*	19	6	6.118	(2)	0.580	2.383	0.7446	0.9985	6.858×10^{-6}	$[\rightarrow {}^{18}\text{C}]$	–
20C	20	6	5.961	1	2.98	2.391	0.8019	1.268	5.646×10^{-6}	5.646×10^{-6}	0.0001285

yields. Higher mass clusters are suppressed by nucleation kinetics and/or size effects.

We are interested in an optimal description of the primary equilibrium distribution at scission. Within a quantum statistical approach, excited bound states and continuum correlations are taken into account. In particular, we have searched for in-medium effects going beyond a simple statistical model of noninteracting components (ideal gas). These in-medium effects are determined by the thermodynamic parameters of matter in the scission region. For all nuclei $Z \leqslant 2$, the Lagrange parameter values are: $\lambda_T = 1.29$, $\lambda_n = -3.09$, $\lambda_p = -16.19$ MeV, volume 1796 fm^3, neutron density $n_n = 6.7 \times 10^{-5}$ fm^{-3}. We showed that for those parameter values, density effects are expected and are manifested by the experimental data.

In particular we find evidence for the Mott effect for the weakly bound states ^{11}Li and ^{19}C, and also the suppression of the yields for weakly bound nuclei ^{6}He, ^{11}Be, ^{14}B, and ^{15}C − ^{17}C (excited states). This shows the consistency of our approach: the nucleon density 6.7×10^{-5} fm^{-3} inferred from composition is also seen in the in-medium shifts, the weakly bound clusters serving as test probes. We identify the strong suppression of ^{11}Li and ^{19}C as a signature of the Mott effect and find that other isotopes are not dissolved so that we find an estimate for the Pauli blocking effect and the corresponding interval of density.

We also considered a generalized relativistic mean-field approach to study the in-medium modifications on light cluster properties, introducing a modification on the scalar cluster-meson coupling. At the low nucleon densities considered here, no significant changes in the yield distribution of isotopes and the nuclear-matter parameter values have been observed. This underlines the validity of the parameter values for temperature, nucleon density, and proton fraction, presented in this paper, to describe nuclear matter in the neck region at scission.

The improved description of nuclear matter at scission conditions is of interest for the properties of neutron-rich astrophysical systems [21,23,25,50–55], for instance, the equation of state, heat capacity, and the neutrino opacity at similar thermodynamic parameter values.

APPENDIX A: EXCITED-STATE MULTIPLIER AND INTRINSIC PARTITION FUNCTION

The contribution of excited states to the intrinsic partition function of a particular channel $\{A, Z\}$, which after expansion
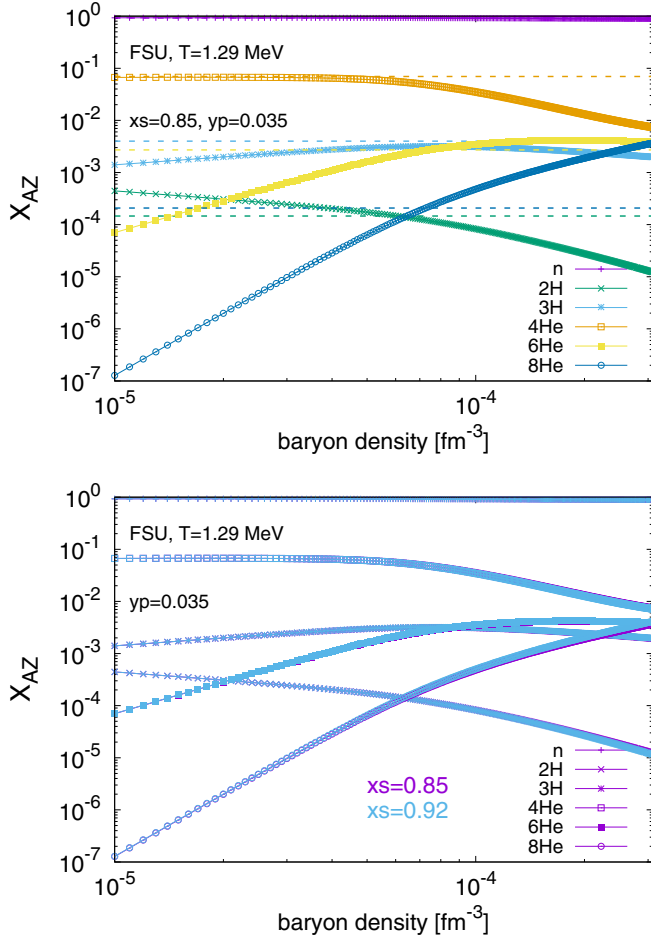
FIG. 5. (Top) Mass fractions as a function of the density for the $Z = 1, 2$ isotopes and the free neutron gas in a RMF calculation with in-medium effects ($x_s = 0.85$) for the FSU model with a fixed temperature of $T = 1.29$ MeV, and a proton fraction of $Y_p = 0.035$. The observed experimental yields are represented by horizontal dotted lines. (Bottom) Mass fractions of the light particles as a function of the density in a RMF calculation employing different values of the scalar cluster-meson coupling constant.
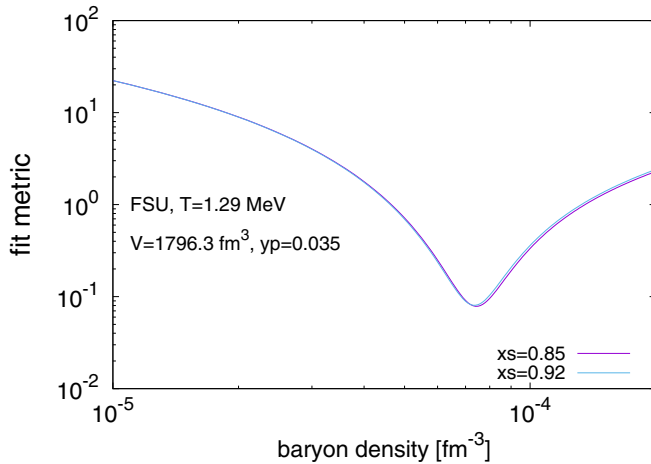

FIG. 6. Fit metric (3) vs. baryon density for $T = 1.29$ MeV and $Y_p = 0.035$, using different values of the scalar cluster-meson coupling.

(feed down) decays to a different final isotope, observed in experiment (branching ratio), is denoted by "*". We separate also the weakly bound states, which are within 1 MeV below the edge of continuum. We denote it by "0" below. Sometimes we separate the ground state so that "0" appears twice.

The threshold energy E_{AZ}^{thresh} is generally given by the neutron separation energy, but lower threshold energies may appear for other decompositions, for instance $^6\text{Li} \rightarrow \alpha + d$ and $^7\text{Li} \rightarrow \alpha + t$, see Ref. [56]. This defines feed-down channels and the corresponding subdivisions of the intrinsic partition function.

The corresponding partition function multipliers $R_{A,Z}^{\text{res.gas}}(\lambda_T)$ and $R_{A,Z}^{\text{vir}}(\lambda_T)$ are calculated for $\lambda_T = 1.29$ MeV. $R_{A,Z}^{\text{medium}}(\lambda_T)$ is calculated for $\lambda_T = 1.29$ MeV, $\lambda_n = -3.09$ MeV, and $\lambda_p = -16.19$ MeV, we indicate only the value for λ_T. See also the Supplemental Material of Ref. [20].

1. $Z \leqslant 2$: n, H, He

Excited states and intrinsic partition function multipliers R of H and He isotopes are shown in Table IV. The contribution of excited states, which, after freezeout, decays to a different channel $\{A, Z\}$ (feed down) is denoted by "*". At low temperatures considered in this work, the subnuclear excitations of the nucleons n, p are neglected so that $R_{1,0} = R_{1,1} = 1$.

2. Lithium

The yields of Li isotopes are shown in Table V. We consider $6 \leqslant A \leqslant 12$ The degeneracy is not known for ^{10}Li and ^{12}Li, the value 3 was assumed, but is not of relevance for the discussion here. The same holds also for some excited states. The threshold energy E_{AZ}^{thresh} is given in general by the neutron separation energy, but lower threshold energies appear for $^6\text{Li} \rightarrow \alpha + d$ and $^7\text{Li} \rightarrow \alpha + t$, see Ref. [56].

3. Beryllium

Results for Be isotopes are shown in Table VI. For the relevant, primary distribution we have to consider also the unstable, excited states. Excited states above the continuum edge, which emit a neutron or other nuclei, are taken separately, their contribution to the intrinsic partition function is denoted by an asterisk. Also excited states little below the continuum edge (1 MeV) may become dissolved in a dense medium if the binding energy is reduced owing to Pauli blocking, their contribution is denoted by "0".

4. Boron

Results for B isotopes are shown in Table VII. As before, we denoted the weakly bound part of the intrinsic partition function with $^{10}\text{B}^0$, $^{12}\text{B}^0$, and $^{14}\text{B}^0$. ^{16}B feeds ^{15}B, and ^{18}B feeds ^{17}B. It is expected that continuum correlations and in-medium effects may give further corrections to describe the final yields of the isotopes.

5. Carbon

For carbon, several states are close to the edge of the continuum, see Table VIII. In particular, ^{19}C is weakly bound, as

is ^{17}C, with the threshold of the continuum below 1 MeV. We expect that these weakly bound nuclei are stronger influenced by in-medium modifications, in particular Pauli blocking.

APPENDIX B: ESTIMATE FOR THE PAULI BLOCKING SHIFT

There are two contributions to the in-medium shift of quasiparticles, the self-energy contribution and the Pauli blocking effects. Self-energy shifts are calculated, e.g., by the relativistic mean-field approximation. If the momentum dependence of the shift is neglected, each nucleon suffers the same shift so that it can be implemented in the chemical potential. The composition is not influenced. For a more detailed discussion see Refs. [31,39].

We give an estimate for the Pauli blocking $\Delta E_{A,Z}^{\text{Pauli}}(\mathbf{P}; T, n_B, Y_p)$ as function of total momentum $\hbar\mathbf{P}$ and the thermodynamic variables T, μ_n, μ_p, respectively, T, n_B, Y_p as

$$\Delta E_{A,Z}^{\text{Pauli}}(\mathbf{P}; T, n_B, Y_p) = e^{-\frac{\hbar^2 P^2}{2A^2 mT}} 2\,(Nn_n + Zn_p)a_{A,Z}e^{-b_{A,Z}T}$$
(B1)

according to Eq. (21) in Ref. [19], where also values for the parameters $a_{A,Z}, b_{A,Z}$ are given. An average value for $10 \leqslant A \leqslant 16$ is $\bar{a} = 532.0$ MeV fm^3 and $\bar{b} = 0.05103$ MeV^{-1}. The $\mathbf{P}$ dependence is according to Eq. (43) of Ref. [31].

Within an exploratory calculation, we use the average value to estimate the Pauli blocking shift. Values for $\Delta E_{A,Z}^{\text{Pauli}}(\mathbf{P} = 0; T, n_B, Y_p) = \Delta E_{A,Z}^{\text{Pauli}}(0)$ are shown in Tables IX, X. The Mott condition where the Pauli blocking shift exceeds the binding energy is fulfilled for ^{11}Li and ^{19}C, but also for excited states of ^{11}Be, ^{14}B, ^{15}C, ^{16}C, and ^{17}C. Further ground states and excited states, denoted by "0", are also approaching the continuum edge and partially suppressed.

The Mott condition does not mean that all clusters of the corresponding state are dissolved. The transition to the continuum gives also a contribution like a resonance, see the case of ^{2}H. An important point is that the Pauli blocking depends on the total momentum $\hbar\mathbf{P}$, see Ref. [39]. For $\Delta E_{A,Z}^{\text{Pauli}}(0) \geqslant B_{A,Z}$, the Mott momentum follows as

$$P^{\text{Mott}} = \left\{ 2A^2 \frac{Tm}{\hbar^2} \ln\left[\frac{\Delta E_{A,Z}^{\text{Pauli}}(0)}{B_{A,Z}}\right] \right\}^{1/2}.$$
(B2)

Not only the high-momentum bound states but also part of the continuum states may evolve to the ground state in the final distribution. However, this leads to the discussion of branching ratios for the reaction network describing the evolution from freezeout to the final observed yields, which is beyond the scope of the present work.

APPENDIX C: EVALUATION OF THE INTRINSIC PARTITION FUNCTION MULTIPLIERS R: VIRIAL APPROXIMATION

In (1), the intrinsic partition function multiplier was introduced as a correction to the simple ideal gas approximation where for each isotope $\{A, Z\}$ only the ground state was considered. However, for each channel we have to consider the

intrinsic partition function, in particular the account of all excited states. The resonance-gas approximation (2) considers all excited, including unstable, states, also resonances in the continuum.

A systematic description of correlations in the continuum is given by the virial approximation. We repeat: we perform a cluster expansion for the interacting system [19], and partial densities of different clusters $\{A, Z\}$ are introduced. The relevant yields $Y_{A,Z}^{\text{rel,vir}}$ in the virial approximation are calculated as

$$Y_{A,Z}^{\text{rel,vir}} \propto g_{A,Z}\left(\frac{2\pi\hbar^2}{Am\lambda_T}\right)^{-3/2} e^{(B_{A,Z} + (A-Z)\lambda_n + Z\lambda_p)/\lambda_T}\,R_{A,Z}^{\text{vir}}(\lambda_T)$$
(C1)

(nondegenerate limit), where $B_{A,Z}$ denotes the (ground-state) binding energy and $g_{A,Z}$ the degeneracy [33]. The factor

$$R_{A,Z}^{\text{vir}}(\lambda_T) = 1 + \sum_i^{\text{exc}} [g_{AZ,i}/g_{A,Z}]e^{-E_{AZ,i}/\lambda_T}$$
(C2)

is related to the intrinsic partition function of the cluster $\{A, Z\}$. The index i characterizes further quantum numbers of the excited state such as angular momentum. The summation is performed over all excited states of excitation energy $E_{AZ,i}$ and degeneracy $g_{AZ,i}$ [33].

As already discussed for H, He, we have also to consider the scattering states. This leads to a change in the contributions obtained for bound states, and, in particular, for the unbound states. We use the Beth-Uhlenbeck relation, see Ref. [18] to perform the sum over the continuum states,

$$C_{AZ,i}^{\text{vir}}(\lambda_T) = \left[1 - e^{-(E_{A,Z}^{\text{thresh}} - E_{AZ,i})/\lambda_T}\right]\Theta\!\left(E_{A,Z}^{\text{thresh}} - E_{AZ,i}\right)$$
$$+ \frac{1}{\pi\lambda_T} e^{-(E_{A,Z}^{\text{thresh}} - E_{AZ,i})/\lambda_T} \int_0^\infty dE\, e^{-E/\lambda_T}\delta_{AZ,i}(E),$$
(C3)

as prefactor for the contribution of the different channels $\{A, Z, i\}$, degeneracy $g_{AZ,i}$. $E_{A,Z}^{\text{thresh}}$ is the difference of the binding energy of the ground state and the binding energy of the components of the lowest continuum, the Θ function is 1 if a bound state occurs. If a channel has no common bound state, we have $E_{AZ,i} = 0$, all excited states are in the continuum. The intrinsic partition function multiplier $R_{A,Z}^{\text{vir}}(\lambda_T)$ (C2) can be rewritten as

$$R_{A,Z}^{\text{vir}}(\lambda_T) = \sum_i^{\text{exc}} \frac{g_{AZ,i}}{g_{A,Z}}e^{-E_{AZ,i}/\lambda_T}C_{A,Z}^{\text{vir}}(\lambda_T, E_{AZ,i}).$$
(C4)

As in the case of the resonance-gas approximation, the sum over all states i can be subdivided into different contributions α,

$$R_{A,Z}^{\text{vir}}(\lambda_T) = \sum_\alpha R_{A,Z}^{\text{vir},\alpha}(\lambda_T).$$
(C5)

We divided it into the contribution of well-bound nuclear states with binding energy larger than 1 MeV (R) and weakly bound states, (R^0), both decaying to the ground state, and in unbound states (R^*), which feed down to other channels. The

same subdivision has been performed also for the intrinsic partition function multiplier $R_{A,Z}^{\text{res.gas}}(\lambda_T)$. We perform this subdivision to calculate the feed-down process from freezeout to the final yields.

We are not able here to evaluate the integral over the scattering phase shifts for all channels of interest. We give only an estimate in analogy of the cases ^{2}H, ^{4}H, ^{5}He, which have been discussed in Ref. [19]. The relation $R_{AZ}^{\text{vir}}(T) = e^{(E_{A,Z}^{\text{thresh}} - E^{\text{eff}}(T))/T}$ was given there. We use the effective energy $E^{\text{eff}}(T)$ given there and have for ^{4}H ($S_n = -1.6$ MeV) the value $R_{^4\text{H}}^{\text{vir}}(1.29) = 0.057$, and for ^{5}He for $S_n = -0.735$ MeV the value $R_{^5\text{He}}^{\text{vir}}(1.29) = 0.731$. Together with the known virial coefficient in the deuteron channel, in Ref. [18] the interpolation formula (in units of MeV)

$$C_{A,Z}^{\text{vir}}(\lambda_T, E_{AZ,i}) = \frac{1}{e^{-(E_{A,Z}^{\text{thresh}} - E_{AZ,i} + 1.129)/0.204} + 1}$$
$$\times \frac{1}{e^{-(E_{A,Z}^{\text{thresh}} - E_{AZ,i} + 2.45)/\lambda_T} + 1} \quad \text{(C6)}$$

has been introduced, which reproduces the values for ^{2}H, ^{4}H, and ^{5}He at $\lambda_T = 1.29$ MeV. If we have multiple contributions within a group α we replace $C_{AZ,i}^{\text{vir}}(\lambda_T, E_{AZ,i})$ by its value for the lowest excitation energy $E_{AZ,\alpha}$ of the group, and can extract this factor from the summation so that

$$R_{A,Z}^{\text{vir},\alpha}(\lambda_T) = C_{A,Z}^{\text{vir}}(\lambda_T, E_{AZ,\alpha}) R_{A,Z}^{\text{res.gas},\alpha}(\lambda_T). \quad \text{(C7)}$$

We used this expression to calculate the multipliers $R_{A,Z}^{\text{vir},\alpha}(\lambda_T)$ shown in the Tables.

APPENDIX D: EVALUATION OF THE INTRINSIC PARTITION FUNCTION MULTIPLIERS R: MEDIUM MODIFICATIONS

The virial expression uses the bound-state energies and scattering phase shifts of the free clusters, neglecting interaction effects. The most important in-medium effects are self-energy and Pauli blocking. Self-energy effects are well known and are parametrized, for instance, as Skyrme forces or relativistic mean-field approximation. If we neglect the momentum dependence of the single-particle mean-field shift, this self-energy shift Δ_τ^{SE} for neutron and protons, which occurs also in the bound states may be included in the effective chemical potentials $\tilde{\lambda}_\tau = \lambda_\tau - \Delta_\tau^{\text{SE}}$. Values for Δ_τ^{SE} have been given in Sec. IV C. Thus, it has no influence on the composition at given temperature and densities.

In contrast, the Pauli blocking shift occurs only for interacting nucleons in a cluster and depends strongly on the quantum state, as discussed above. Therefore we take this shift of energy levels explicitly into account. In principle, also the scattering phase shifts are modified. See Ref. [29] for the two-nucleon case, where a generalized Beth-Uhlenbeck approach is given, which accounts for in-medium effects.

The Pauli blocking has different consequences. (i) In (C1), (C2), the energy shift of the bound states $\Delta E_{A,Z,i}^{\text{Pauli}}$ has to be added to the binding energies $B_{A,Z}^{\text{medium}} = B_{A,Z} - \Delta E_{A,Z}^{\text{Pauli}}$ for the ground state, but also for all excitation energies $E_{AZ,i}^{\text{medium}} =$

$E_{AZ,i} + \Delta E_{A,Z,i}^{\text{Pauli}} - \Delta E_{A,Z}^{\text{Pauli}}$, which are taken relatively to the ground state. In principle, the Pauli blocking depends on the wave function of the bound state as well as the total momentum $\mathbf{P}$ of the cluster, but for simplicity we assume that we can neglect this and approximate these different Pauli blocking shifts by $\Delta E_{A,Z}^{\text{Pauli}}$. Then, a common factor can be extracted so that $e^{-\Delta E_{A,Z}^{\text{Pauli}}/\lambda_T} R_{A,Z}^{\text{vir}}(\lambda_T)$ appears.

(ii) The medium modifications will also result in a density dependence of the intrinsic partition function or the corresponding factors $R_{A,Z}^{\text{medium},\alpha}(T, n_B, Y_p)$ in the decomposition corresponding to Eq. (C7). We use the virial expression (C7) but replace in $C_{A,Z}^{\text{vir}}(\lambda_T, E_{AZ,\alpha})$ the excitation energy $E_{AZ,\alpha}$ by $E_{AZ,\alpha} + \Delta E_{A,Z}^{\text{Pauli}}$,

$$R_{A,Z}^{\text{medium},\alpha}(\lambda_T, \lambda_n, \lambda_p) = C_{AZ}^{\text{vir}}(\lambda_T, E_{AZ,\alpha} + \Delta E_{A,Z}^{\text{Pauli}})$$
$$\times R_{A,Z}^{\text{res.gas},\alpha}(\lambda_T) e^{-\Delta E_{A,Z}^{\text{Pauli}}/\lambda_T}. \quad \text{(D1)}$$

The shift of the bound states gives a decrease of the binding energy. which may vanish (Mott effect). The dissolution of bound states opens additional channels for feed-down processes.

We discuss three different cases: well bound states with binding energy larger than $T \approx 1$ MeV are shifted but not dissolved. Because the temperature is low, the effect of continuum correlations and the threshold energy is small for the strongly bound isotopes so that, in addition to the self-energy shift $\Delta_{A,Z}^{\text{SE}}$, the factor $\exp[-\Delta E_{A,Z}^{\text{Pauli}}/\lambda_T]$ determines the influence of the medium. The contribution of scattering states has been approximated by Eq. (C6), replacing $E_{AZ,i}$ by $E_{AZ,i} + \Delta E_{AZ,i}^{\text{Pauli}}$.

Of special interest are the weakly bound states where the shift brings it above the continuum edge, $E_{AZ,i} + \Delta E_{A,Z}^{\text{Pauli}} - E_{AZ}^{\text{thresh}} > 0$ so that the bound state will be dissolved and feed down other final states. We estimate these contributions also according to Eq. (C6) as done above for the scattering states. Instead to feed down the ground state after deexcitation, we assume that they feed down other isotopes as indicated in Tables IX, X.

This simplified picture to describe the reaction processes after freezeout has to be improved in future treatments within a systematic nonequilibrium approach. As known from reaction networks describing expanding matter in astrophysics, branching ratios may be introduced to describe the evolution of the primary distribution to the final distribution, which allow for different final states of an excited state. For our considerations this is not of relevance as long as the contribution of excited states (including continuum states) is small, and the main contribution to the yield of isotopes is determined by the strongly bound states. Another situation appears for the weakly bound final states such as ^{11}Li and ^{19}C in our calculation, see Tables IX, X. Because they are shifted to the continuum, in our simple treatment of the feed-down process they will feed other isotopes, and the final yield for both isotopes will be zero. A more detailed description would allow that some of the primary states may remain in the bound state. For instance, the Pauli blocking is momentum dependent, and clusters with large momentum remain bound because Pauli blocking is effective only within the Fermi

sphere, as discussed in Sec. B and Sec. IV C. There is also a finite probability that continuum contributions according to the Beth-Uhlenbeck formula will deexcite to the ground state according to a coalescence model. For this one has to introduce branching ratios, which allow feed down to different final states. Even being small, special feed-down processes become visible if they are the only process to form a final bound state.

We are not able in this work to derive a microscopic expression for the branching ratios during expansion after freezeout. They are of relevance when they are the only process to populate the final yield, for instance, of the dissolved isotopes ^{11}Li and ^{19}C in Tables IX, X. To give an example, we assumed in both cases a branching ratio 0.1 that the primary yield remains

at the same isotope to form the final yield. As shown in Fig. 4, this branching ratio would fit the yield of ^{19}C to the general behavior of the calculated yields. This example is only for illustration, the derivation of the branching ratio goes beyond the frame of the present work.

Another issue that needs further considerations is the threshold energy $E_{A,Z}^{\text{thresh}}$, which is taken in this work from the data tables. It is possible that this quantity is also changed in a dense medium. For this, a nonequilibrium approach to the reaction processes is necessary, which finally will provide us with in-medium branching ratios discussed above. Our description of the reactions during the expansion process after freezeout remains a semiempirical one with a simplified reaction network as shown in Tables IX, X.

---

[1] I. Halpern, Ann. Rev. Nucl. Sci. **21**, 245 (1971).

[2] C. Wagemans, *The Nuclear Fission Process* (CRC Press, Boca Raton, 1991), and references therein.

[3] R. W. Mills, Thesis, University of Birmingham, 1995.

[4] IAEA-TECDOC-1168: Compilation and evaluation of fission yield nuclear data, Final report of a coordinated research project 1991–1996, and references therein.

[5] H. J. Krappe and K. Pomorski, *Theory of Nuclear Fission (Lecture Notes in Physics)* (Springer, Heidelberg, 2012), Vol. 383.

[6] A. Schubert *et al.*, Z. Phys A **341**, 481 (1992).

[7] A. S. Vorobyev *et al.*, J. Exp. Theor. Phys. **127**, 659 (2018).

[8] I. S. Guseva *et al.*, Phys. At. Nucl. **81**, 447 (2018).

[9] U. Koester *et al.*, Nucl. Phys. A **652**, 371 (1999).

[10] U. Koester, PhD thesis, Technische Universität München, 2000.

[11] Yu. N. Kopatch, M. Mutterer, D. Schwalm, P. Thirolf, and F. Gönnenwein, Phys. Rev. C **65**, 044614 (2002).

[12] G. V. Val'skii, Yad. Fiz. **24**, 270 (1976) [Phys. Atom. Nuclei **67**, 1264 (2004)].

[13] J. P. Lestone, Int. J. Mod. Phys. E **17**, 323 (2008).

[14] S. Wuenschel, H. Zheng, K. Hagel, B. Meyer, M. Barbui, E. J. Kim, G. Ropke, and J. B. Natowitz, Phys. Rev. C **90**, 011601(R) (2014).

[15] J. Schmelzer, G. Röpke, and F. P. Ludwig, Phys. Rev. C **55**, 1917 (1997).

[16] P. Demo and Z. Kozisek, J. Phys. G: Nucl. Part. Phys. **23**, 971 (1997).

[17] J. B. Natowitz, H. Pais, G. Röpke, J. Gauthier, K. Hagel, M. Barbui, and R. Wada, Phys. Rev. C **102**, 064621 (2020).

[18] G. Röpke, J. B. Natowitz, and H. Pais, Eur. Phys. J. A **56**, 238 (2020).

[19] G. Röpke, Phys. Rev. C **101**, 064310 (2020).

[20] G. Röpke, J. B. Natowitz, and H. Pais, Phys. Rev. C **103**, L061601 (2021).

[21] M. V. Beznogov, D. Page, and E. Ramirez-Ruiz, Astrophys. J. **888**, 97 (2020).

[22] A. Arcones, G. Martínez-Pinedo, E. O'Connor, A. Schwenk, H.-Th. Janka, C. J. Horowitz, and K. Langanke, Phys. Rev. C **78**, 015806 (2008).

[23] T. Fischer, S. C. Whitehouse, A. Mezzacappa, F. K. Thielemann, and M. Liebendorfer, Astron. Astrophys. **517**, A80 (2010).

[24] M. Oertel, M. Hempel, T. Klähn, and S. Typel, Rev. Mod. Phys. **89**, 015007 (2017).

[25] S. Furusawa and H. Nagakura, Prog. Part and Nucl. Phys. **129**, 104018 (2023).

[26] G. Röpke, L. Münchow, and H. Schulz, Nucl. Phys. A **379**, 536 (1982).

[27] M. Hempel and J. Schaffner-Bielich, Nucl. Phys. A **837**, 210 (2010).

[28] M. Hempel, K. Hagel, J. Natowitz, G. Röpke, and S. Typel, Phys. Rev. C **91**, 045805 (2015).

[29] M. Schmidt *et al.*, Ann. Phys. (NY) **202**, 57 (1990).

[30] C. J. Horowitz and A. Schwenk, Nucl. Phys. A **776**, 55 (2006).

[31] G. Röpke, Phys. Rev. C **79**, 014002 (2009).

[32] S. Typel, G. Röpke, T. Klahn, D. Blaschke, and H. H. Wolter, Phys. Rev. C **81**, 015803 (2010).

[33] Data tables of nuclei Nudat 2: https://www.nndc.bnl.gov/nudat2/.

[34] G. Röpke, Phys. Rev. C **92**, 054001 (2015).

[35] M. Andronenko *et al.*, Eur. Phys. J. A **12**, 185 (2001).

[36] M. Popkiewicz *et al.*, https://www.osti.gov/etdeweb/servlets/purl/583067, 1996

[37] U. Koester *et al.*, *Proceedings from the Pont d'Oye IV Conference*, October 6–8, 1999, Habay-la-Neuve, Belgium, pp. 1–16.

[38] S. Typel, Phys. Rev. C **71**, 064301 (2005).

[39] G. Röpke, Nucl. Phys. A **867**, 66 (2011).

[40] H. Pais, F. Gulminelli, C. Providencia, and G. Ropke, Phys. Rev. C **97**, 045805 (2018).

[41] B. G. Todd-Rutel and J. Piekarewicz, Phys. Rev. Lett. **95**, 122501 (2005).

[42] M. D. Voskresenskaya and S. Typel, Nucl. Phys. A **887**, 42 (2012).

[43] C. J. Horowitz and A. Schwenk, Phys. Lett. B **638**, 153 (2006).

[44] L. Qin *et al.*, Phys. Rev. Lett. **108**, 172701 (2012).

[45] H. Pais, F. Gulminelli, C. Providencia, and G. Ropke, Phys. Rev. C **99**, 055806 (2019).

[46] S. Burrello and S. Typel, Eur. Phys. J. A **58**, 120 (2022).

[47] C. J. Yang, M. Grasso, and D. Lacroix, Phys. Rev. C **94**, 031301(R) (2016).

[48] M. Grasso, D. Lacroix, and C. J. Yang, Phys. Rev. C **95**, 054327 (2017).

[49] H. Pais *et al.*, Phys. Rev. Lett. **125**, 012701 (2020); J. Phys. G. **47**, 105204 (2020).

[50] F. Gulminelli and Ad. R. Raduta, Phys. Rev. C **92**, 055803 (2015).

[51] S. Burrello, F. Gulminelli, F. Aymard, M. Colonna, and Ad. R. Raduta, Phys. Rev. C **92**, 055804 (2015).

[52] S. Burrello, M. Colonna, and F. Matera, Phys. Rev. C **94**, 012801(R) (2016).

[53] Y. Lim and J. W. Holt, Phys. Rev. C **95**, 065805 (2017).

[54] X. Du, A. W. Steiner, and J. W. Holt, Phys. Rev. C **105**, 035803 (2022).

[55] A. Sedrakian, Eur. Phys. J. A **56**, 258 (2020).

[56] P. Jesinger *et al.*, Eur. Phys. J. A **24**, 379 (2005).